Chapter 3
Velocity Field and Pressure Drop in Single-Phase Flows

The available experimental data on the flow of incompressible fluids are generalized. These data encompass a wide range of Reynolds numbers that correspond to laminar, transient and turbulent regimes of the flow. Thermal effects due to energy dissipation are estimated. Laminar drag reduction in micro-channels using hydrophobic surfaces is discussed. Data of experimental investigations related to the flow in smooth and rough micro-channels are compared with predictions of the conventional theory. Possible sources of divergence of experimental and theoretical results are also discussed.

3.1 Introduction

Flow in small tubes has been studied by many researchers over the years. Schlichting (1979) documents the then-available theories and experimental data, starting with the pioneering works by Hagen (1839) and Poiseuille (1840). Rapid development of micro-mechanics stimulated during the last decades numerous investigations in the field of fluid mechanics of micro-devices (Ho and Tai 1998; Gad-el-Hak 1999; Bayraktar and Pidugu 2006). Research in this field is important for different applications in micro-system technology, in particular, micro-scaled cooling systems of electronic devices, which generate high power (Tuckerman 1984; Incropera 1999).

The problems of micro-hydrodynamics were considered in different contexts: (1) drag in micro-channels with a hydraulic diameter from 10^6 m to 10^3 m at laminar, transient and turbulent single-phase flows, (2) heat transfer in liquid and gas flows in small channels, and (3) two-phase flow in adiabatic and heated micro-channels. The studies performed in these directions encompass a vast class of problems related to flow of incompressible and compressible fluids in regular and irregular micro-channels under adiabatic conditions, heat transfer, as well as phase change.

L.P. Yarin, *Fluid Flow, Heat Transfer and Boiling in Micro-Channels*

In spite of the existence of numerous experimental and theoretical investigations, a number of principal problems related to micro-fluid hydrodynamics are not well-studied. There are contradictory data on the drag in micro-channels, transition from laminar to turbulent flow, etc. That leads to difficulties in understanding the essence of this phenomenon and is a basis for questionable discoveries of special "micro-effects" (Duncan and Peterson 1994; Ho and Tai 1998; Plam 2000; Herwig 2000; Herwig and Hausner 2003; Gad-el-Hak 2003). The latter were revealed by comparison of experimental data with predictions of a conventional theory based on the Navier–Stokes equations. The discrepancy between these data was interpreted as a display of new effects of flow in micro-channels. It should be noted that actual conditions of several experiments were often not identical to conditions that were used in the theoretical models. For this reason, the analysis of sources of disparity between the theory and experiment is of significance.

We attempt here to reveal the actual reasons of disparity between the theoretical predictions and measurements obtained for single-phase flow in micro-channels. For this purpose, we consider the effect of different factors (roughness, energy dissipation, etc.) on flow characteristics. Some of these factors were also discussed by Sharp et al. (2001), and Sharp and Adrian (2004).

We consider the problem of liquid and gas flow in micro-channels under the conditions of small Knudsen and Mach numbers that correspond to the continuum model. Data from the literature on pressure drop in micro-channels of circular, rectangular, triangular and trapezoidal cross-sections are analyzed, whereas the hydraulic diameter ranges from 1.01 to 4,010 μm. The Reynolds number at the transition from laminar to turbulent flow is considered. Attention is paid to a comparison between predictions of the conventional theory and experimental data, obtained during the last decade, as well as to a discussion of possible sources of unexpected effects which were revealed by a number of previous investigations.

This chapter has the following structure: in Sect. 3.2 the common characteristics of experiments are discussed. Conditions that are needed for proper comparison of experimental and theoretical results are formulated in Sect. 3.3. In Sect. 3.4 the data of flow of incompressible fluids in smooth and rough micro-channels are discussed. Section 3.5 deals with gas flows. The data on transition from laminar to turbulent flow are presented in Sect. 3.6. Effect of measurement accuracy is estimated in Sect. 3.7. A discussion on the flow in capillary tubes is given in Sect. 3.8.

3.2 Characteristics of Experiments

For the analysis of flow in micro-channels we use the following experimental data:

1. Smooth micro-channels by Li et al. (2003), Yang et al. (2003), Pfund et al. (2000), Xu et al. (2000), Wu and Cheng (2003), Maynes and Webb (2002), Judy et al. (2002), Sharp and Adrian (2004), and Celata et al. (2006)

2. Micro-channels with roughness by Peng and Peterson (1996), Peng and Wang (1998), Mala and Li (1999), Qu et al. (2000), Pfund et al. (2000), Li et al. (2003), and Kandlikar et al. (2003)
3. Transition from laminar to turbulent flow by Peng and Peterson (1996), Peng and Wang (1998), Pfund et al. (2000), Li et al. (2003) and Sharp and Adrian (2004)
4. Gas flow in micro-channels by Harley et al. (1995), and Hsieh et al. (2004)

Brief characteristics of these experiments are given in Table 3.1. The flow characteristics (flow rate, pressure gradient, average and fluctuating velocities) were measured for flow in micro-channels, both smooth and with roughness, of different geometry. The physical properties of the fluids used in the experiments, as well as the material of the micro-channel walls varied widely, which allows for analyzing the effect of fluid composition, in particular, the ionic component, as well as the influence of fluid–wall interaction, on the flow characteristics. The Reynolds number in the experiments varied in the range $10^3 < \mathrm{Re} < 4 \times 10^3$, which covers the regimes of laminar, transition and turbulent flow. An extremely large relative length of micro-channels is characteristic for the considered experiments: $10^2 < L/d_* < 15 \times 10^4$, where L is the length of the micro-channel and d_* is the characteristic dimension of diameter or depth for circular or rectangular micro-channels, respectively.

In general, conventional theory has been tested for flow in micro-channels by comparing the experimental and theoretical data on pressure drop as a function of flow rate. During the last few years, better methods have been used for measurement of the mean velocity, as well as rms of the velocity fluctuations (Maynes and Webb 2002; Sharp and Adrian 2004).

Table 3.1 Flow characteristics in micro-channels

Geometry of the tube		Circular, Rectangular, Trapezoidal, Triangular
Size	d_h μm	$3\text{–}4 \times 10^3$
	h μm	0.51–250
$\frac{L}{d_*}$		$90\text{–}15 \times 10^4$
Wall	Material	Glass, Silica, Stainless steel
	Surface	Smooth, Rough
Fluid	Liquid	Tap water, Dist. water, De-ion. water, R-134a, Methanol, Isopropanol, Carbon tetrachloride solutions with several ionic compositions
	Gas	Air, N_2, He, Ar
Re		$10^3\text{–}4 \times 10^3$
U	m/s	10^4–30
Measured parameter		Flow rate, Pressure gradient, Mean velocity, rms of velocity fluctuations

3.3 Comparison Between Experimental and Theoretical Results

The classical solution of the problem of steady laminar flow in straight ducts is based on a number of assumptions on flow conditions, Hetsroni et al. (2005)

1. The flow is generated by a force due to a static pressure in the fluid.
2. The flow is stationary and fully developed, i.e., it is strictly axial.
3. The flow is laminar.
4. The Knudsen number is small enough so that the fluid is a continuous medium.
5. There is no slip at the wall.
6. The fluids are incompressible Newtonian fluids with constant viscosity.
7. There is no heat transfer to/from the ambient.
8. The energy dissipation is negligible.
9. There is no fluid/wall interaction (except purely viscous).
10. The channel walls are straight.
11. The channel walls are smooth.

In this case the problem of developed laminar flow in a straight duct reduces to integrating the equation

$$\mu\left(\frac{\partial^2 u}{\partial y^2}+\frac{\partial^2 u}{\partial z^2}\right)=\frac{\mathrm{d}P}{\mathrm{d}x} \tag{3.1}$$

with no-slip condition on the contour, which determines the channel shape.

In Eq. (3.1) $u=u(y,z)$ is the velocity component in the longitudinal x-direction, P is the pressure, μ is the dynamic viscosity, and x,y,z are the Cartesian coordinates.

The solution of Eq. (3.1) leads to the following expression for the friction factor

$$\lambda=\frac{\text{const}}{\text{Re}} \tag{3.2}$$

or

$$\text{Po}=\text{const} \tag{3.3}$$

where $\lambda=\frac{2\Delta P}{L}\frac{d_*}{\rho U^2}$ is the friction factor, $\text{Po}=\lambda\cdot\text{Re}$ is the Poiseuille number, and ΔP is the pressure drop on a channel length L, d_* is the characteristic size.

The constant in Eqs. (3.2) and (3.3) is determined by the micro-channel shape and does not depend on the flow parameters, as shown in Table 3.2 (Loitsianskii 1996). In Table 3.2, d is the diameter of the tube, α and β are the semi-axes of the ellipse, a is the side of an equilateral triangle, H is the side of a rectangle, and $f(\xi)$

Table 3.2 Parameters of micro-channels (Loitsianskii 1996)

Shape of micro-channel	Characteristic size	Constant in Eqs. (3.2), (3.3)
Circular	$d_*=d$	64
Elliptical	$d_*=\frac{1}{2\sqrt{2}}\frac{\alpha\beta}{(\alpha^2+\beta^2)^{1/2}}$	64
Equilateral triangular	$d_*=a$	160
Rectangular	$d_*=H$	$128/f(\xi)$

is a tabulated function of height-to-width ratio; $f(\xi)$ changes from 2.253 to 5.333 when ξ varies from 1 to ∞.

The data on pressure drop in irregular channels are presented by Shah and London (1978) and White (1994). Analytical solutions for the drag in micro-channels with a wide variety of shapes of the duct cross-section were obtained by Ma and Peterson (1997). Numerical values of the Poiseuille number for irregular micro-channels are tabulated by Sharp et al. (2001). It is possible to formulate the general features of Poiseuille flow as follows:

$$\frac{\mathrm{d}\,\mathrm{Po}}{\mathrm{d}\,\mathrm{Re}} = 0 \tag{3.4}$$

$$C^* = \frac{\mathrm{Po}_{\mathrm{exp}}}{\mathrm{Po}_{\mathrm{theor}}} \tag{3.5}$$

where C^* is the ratio of the Poiseuille number defined experimentally to the same one defined from theory. $\mathrm{Po}_{\mathrm{exp}}$ and $\mathrm{Po}_{\mathrm{theor}}$ are the experimental and theoretical Poiseuille numbers, respectively.

Equation (3.4) reflects the dependence of the friction factor on the Reynolds number, whereas Eq. (3.5) shows conformity between actual and calculated shapes of a micro-channel. Condition (3.5) is the most general since it testifies to an identical form of the dependencies of the experimental and theoretical friction factor on the Reynolds number.

Basically, there may be three reasons for the inconsistency between the theoretical and experimental friction factors: (1) discrepancy between the actual conditions of a given experiment and the assumptions used in deriving the theoretical value, (2) error in measurements, and (3) effects due to decreasing the characteristic scale of the problem, which leads to changing correlation between the mass and surface forces (Ho and Tai 1998).

3.4 Flow of Incompressible Fluid

3.4.1 Smooth Micro-Channels

We begin the comparison of experimental data with predictions of the conventional theory for results related to flow of incompressible fluids in smooth micro-channels. For liquid flow in the channels with the hydraulic diameter ranging from 10^6 m to 10^3 m the Knudsen number is much smaller than unity. Under these conditions, one might expect a fairly good agreement between the theoretical and experimental results. On the other hand, the existence of discrepancy between those results can be treated as a display of specific features of flow, which were not accounted for by the conventional theory. Bearing in mind these circumstances, we consider such experiments, which were performed under conditions close to those used for the theoretical description of flows in circular, rectangular, and trapezoidal micro-channels.

Glass and silicon tubes with diameters of 79.9–166.3 μm, and 100.25–205.3 μm, respectively, were employed by Li et al. (2003) to study the characteristics of friction factors for de-ionized water flow in micro-tubes in the Re range of 350 to 2,300. Figure 3.1 shows that for fully developed water flow in smooth glass and silicon micro-tubes, the Poiseuille number remained approximately 64, which is consistent with the results in macro-tubes. The Reynolds number corresponding to the transition from laminar to turbulent flow was Re = 1,700−2,000.

Yang et al. (2003) obtained the friction characteristics for air, water, and liquid refrigerant R-134a flow in tubes with inside diameters from 173 to 4,010 μm. The test results showed that the pressure drop correlations for large tubes might be adequately used for water, refrigerant, and low-speed air flow in micro-tubes. The laminar-turbulent transition Reynolds number varied from 1,200 to 3,800 and increased with decreasing tube diameters. The test friction factors agree very well with the Poiseuille equation for the laminar flow regime.

Pfund et al. (2000) studied the friction factor and Poiseuille number for 128–521 μm rectangular channels with smooth bottom plate. Water moved in the channels at Re = 60−3,450. In all cases corresponding to Re < 2,000 the friction factor was inversely proportional to the Reynolds number. A deviation of Poiseuille number from the value corresponding to theoretical prediction was observed. The deviation increased with a decrease in the channel depth. The ratio of experimental to theoretical Poiseuille number was 1.08 ± 0.06 and 1.12 ± 0.12 for micro-channels with depths 531 and 263 μm, respectively.

Xu et al. (2000) investigated de-ionized water flow in micro-channels with hydraulic diameter ranging from 30 to 344 μm at Reynolds numbers ranging from 20 to 4,000. Two test modules were used. The first test module consisted of a cover and an aluminum plate, into which a micro-channel, inlet and outlet sumps were machined. A Plexiglas plate was used to cover the channel. The second module was fabricated from a silicon wafer, and a 5 mm thick Pyrex glass was utilized to

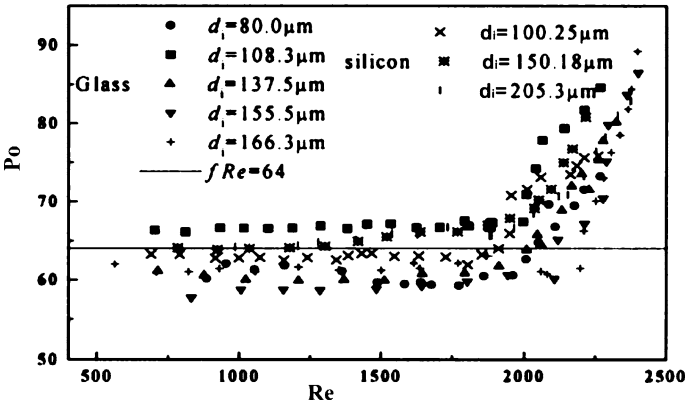

Fig. 3.1 Dependence of the Poiseuille number on the Reynolds number. Reprinted from Li et al. (2003) with permission

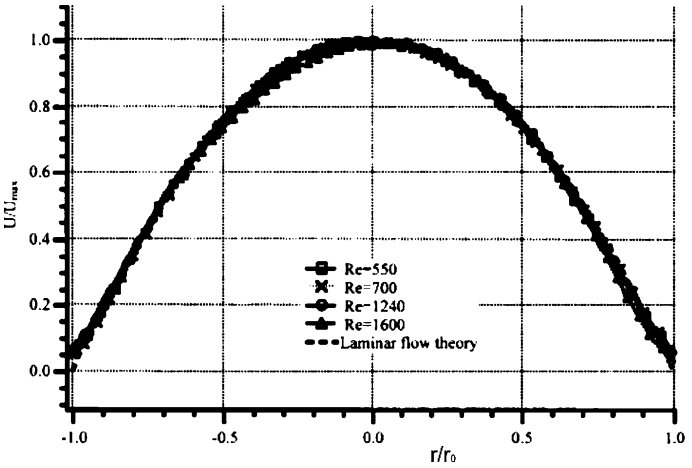

Fig. 3.2 Velocity profiles vs. r/r_0. Reprinted from Maynes and Webb (2002) with permission

cover the channel by using anodic bonding. The experimental data obtained in both modules showed that the trend of water flow in micro-channels is similar to the prediction of the conventional theory as a whole, i.e., that Po = const. for flow in the laminar region. However, some discrepancy between the results obtained in these modules occurred. For flow in the first test module, in which the hydraulic diameter of the channels varied from 50 to 300 μm, the Po values in the channels smaller than 100 μm were lower than those predicted by the theory. This phenomenon did not occur in the second test module. Experimental results there almost agree with the theory for flow in micro-channels varying from 30 to 60 μm. The authors explained the disagreement and showed that the actual dimension of the first module would be inaccurate when the cover and micro-channel plate were sealed by bonding with glue due to the thickness of the layer of the cured material.

The transition to turbulent flow occurred at Re of about 1,500. The authors noted that for smaller micro-channels, the flow transition would occur at lower Re. The early transition phenomenon might be affected by surface roughness and other factors.

Wu and Cheng (2003) measured the friction factor of laminar flow of de-ionized water in smooth silicon micro-channels of trapezoidal cross-section with hydraulic diameters in the range of 25.9 to 291.0 μm. The experimental data were found to be in agreement within $\pm 11\%$ with an existing theoretical solution for an incompressible, fully developed, laminar flow in trapezoidal channels under the no-slip boundary condition. It is confirmed that Navier–Stokes equations are still valid for the laminar flow of de-ionized water in smooth micro-channels having hydraulic diameter as small as 25.9 μm. For smooth channels with larger hydraulic diameters of 103.4–103.4–291.0 μm, transition from laminar to turbulent flow occurred at Re = 1,500−2,000.

Maynes and Webb (2002) presented pressure drop, velocity and rms profile data for water flowing in a tube 0.705 mm in diameter, in the range of Re = 500−5,000. The velocity distribution in the cross-section of the tube was obtained using the molecular tagging velocimetry technique. The profiles for Re = 550, 700, 1,240, and 1,600 showed excellent agreement with laminar flow theory, as presented in Fig. 3.2. The profiles showed transitional behavior at Re > 2,100. In the range Re = 550−2,100 the Poiseuille number was Po = 64.

Lelea et al. (2004) investigated experimentally fluid flow in stainless steel micro-tubes with diameter of 100–500 μm at Re = 50−800. The obtained results for the Poiseuille number are in good agreement with the conventional theoretical value Po = 64. Early transition from laminar to turbulent flow was not observed within the studied range of Reynolds numbers.

Papautsky et al. (1999) investigated the flow friction characteristics of water flowing through rectangular micro-channels with width varying from 150 to 600 μm, height (depth) ranging from 22.71 to 26.35 μm, and relative roughness of 0.00028. The experiments were conducted in the range of extremely low Reynolds numbers, 0.001 < Re < 10. The measurements showed that the ratio C^* was independent of Re. This value was about 1.2, i.e., nearly 20% above the value of C^* corresponding to the conventional theory.

The frictional pressure drop for liquid flows through micro-channels with diameter ranging from 15 to 150 μm was explored by Judy et al. (2002). Micro-channels fabricated from fused silica and stainless steel were used in these experiments. The measurements were performed with a wide variety of micro-channel diameters, lengths, and types of working fluid (distilled water, methanol, isopropanol), and showed that there were no deviations between the predictions of conventional theory and the experiment. Sharp and Adrian (2004) studied the fluid flow through micro-channels with the diameter ranging from 50 to 247 μm and Reynolds number from 20 to 2,300. Their measurements agree fairly well with theoretical data.

Cui et al. (2004) studied the flow characteristics in micro-tubes driven by high pressure ranging from 1 to 30 MPa. The diameters of the micro-tubes were from 3 to 10 μm and de-ionized water, isopropanol and carbon tetrachloride were used as the working fluid. The Reynolds number ranged from 0.1 to 24. The measurements showed that the ratio $C^* = \mathrm{Po}_{\mathrm{exp}}/\mathrm{Po}_{\mathrm{theor}}$ varied slightly with the pressure for de-ionized water. But for the other two liquids, isopropanol and carbon tetrachloride, C^* increased markedly with pressure, as shown in Fig. 3.3. It should be noted that the viscosity is extremely sensitive to the flow temperature. The viscosity of water in the pressure range from 1 to 30 MPa can be approximately regarded as constant. Therefore C^* varied very slightly with pressure. The results of isopropanol and carbon tetrachloride were corrected taking into account the viscosity–pressure relationship to obtain the revised theoretical flow rate and revised normalized friction coefficient. Two revised results for $d = 10$ μm for isopropanol and carbon tetrachloride are shown in Fig. 3.4. It can be seen that the experimental data agree well with theoretical prediction. For $d = 5$ and 3 μm micro-tubes, similar tendencies were observed.

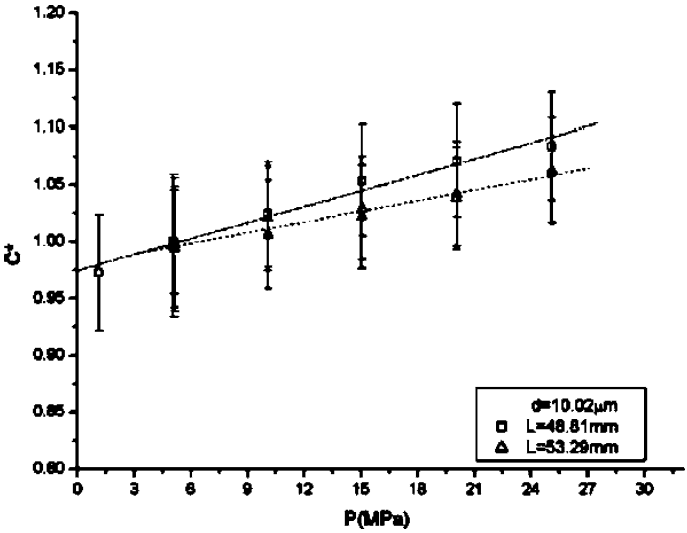

Fig. 3.3 The normalized Poiseuille number as a function of pressure for carbon tetrachloride in 10 μm micro-tube. Reprinted from Cui et al. (2004) with permission

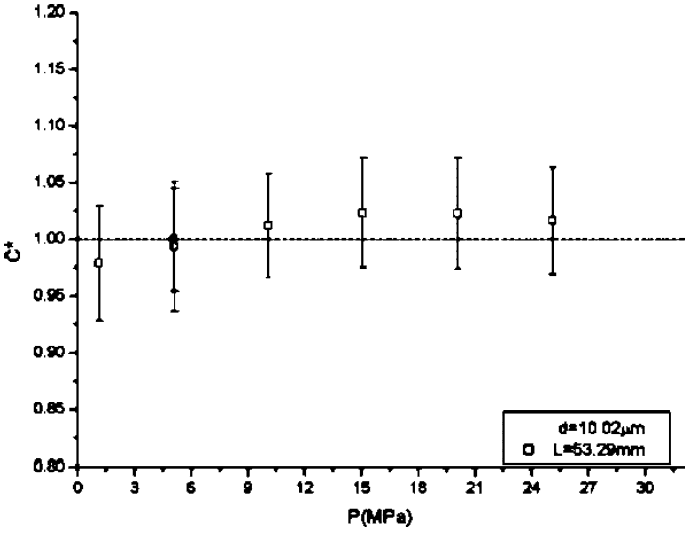

Fig. 3.4 The revised normalized Poiseuille number as a function of pressure for carbon tetrachloride in 10 μm micro-tube. Reprinted from Cui et al. (2004) with permission

Celata et al. (2006) studied experimentally the drag in glass/fused silica microtubes with inner diameter ranging from 31 to 259 μm for water flow with Re $>$ 300. The drag measurements show that the friction factor for all diameters agrees well with predictions of conventional theory: $\lambda = 64/\mathrm{Re}$ (for the smallest diameter 31 μm, the deviations of experimental points from the line $\lambda = 64/\mathrm{Re}$ do not exceed

Table 3.3 Experimental results of single-phase fluid flow in smooth micro-channels

Author	Micro-channel		Fluid	Re	Poiseuille number		Re_{cr}
	Shape	d_h [μm]			$\frac{Po_{exp}}{Po_{theor}}$	Dependence on Re ($Re < Re_{cr}$)	
Sharp, Adrian (2004)	Circular tube	50–245	De-ionized water, 1-propanol and 20% weigh of glycerol solution	20–400 400–2,900	1	Independent	1,800–2,300
Li et al. (2003)	Circular tube	79.9–166.3 100.25–205.5	De-ionized water	350–2,300	1	Independent	1,700–2,000
Yang et al. (2003)	Circular tube	173, 4,010	Water R-134a	1,200–3,800	1	Independent	1,200–3,800
Maynes, Webb (2002)	Circular tube	705	Water	500–5,000	1	Independent	2,200
Judy et al. (2002)	Circular tube square micro-channel	15–150	Distilled water Methanol Isopropanol	8–2,300	1	Independent	$\sim 2{,}000$
Celata et al. (2006)	Circular tube	31–251	Water	300–3,000	1	Independent	2,000–3,000
Lelea et al. (2004)	Circular tube	100, 300, 500	Distilled water	50–800	1	Independent	2,800
Cui et al. (2004)	Circular tube	3–10	De-ionized Isopropanol Carbon tetrachloride	0.1–24	~ 1 (For revised data)		
Hwang, Kim (2006)	Circular tube	244–792	R-134a	200–10,000	1	Independent	$\sim 2{,}000$
Pfund et al. (2000)	Rectangular	128–1,050	Water	60–3,450	1.08–1.12	Independent	1,700–2,200
Xu et al. (2000)	Rectangular	30–344	Clean water	20–4,000	1	Independent	1,500
Papautsky et al. (1999)	Rectangular	Width 150–600 Height 22.71–26.35	Water	0.001–10	1.195	Independent	–
Wu, Chen (2003)	Trapezoidal	25.9–291	De-ionized water		1 ± 0.11	Weak dependent	1,500–2,000

$\pm 19\%$). The transition from laminar to turbulent flow occurs at $2 \times 10^3 < \mathrm{Re} < 3 \times 10^3$.

The experimental results of single-phase flow in smooth micro-channels are summarized in Table 3.3.

3.4.2 Micro-Channels with Rough Walls

Several investigators obtained friction factors in micro-channels with rough walls that were greater than those in smooth wall channels. These observations should be considered taking into account the entrance effects, losses from change in channel size, etc.

The existence of roughness leads also to decreasing the value of the critical Reynolds number, at which transition from laminar to turbulent flow occurs. The character of the dependence of the friction factor on the Reynolds number in laminar flow remains the same for both smooth and rough micro-channels, i.e., $\lambda = \mathrm{const}/\mathrm{Re}$.

The general characteristics of experimental investigations of pressure drop in micro-channels with roughness are presented in Table 3.4. The experiments involve a wide range of flow conditions as related to shape of micro-channels (circular, rectangular, trapezoidal), their sizes ($50\,\mu\mathrm{m} < d_\mathrm{h} < 10^3\,\mu\mathrm{m}$), and the Reynolds numbers ($10^2 < \mathrm{Re} < 4 \times 10^3$). The relative roughness of these micro-channels k_s/r_0 varied from 0.32 to 7%. It is known that hydraulically smooth flow regime occurs when the Reynolds number, which is defined by height of roughness k_s and friction velocity u_*, varies in the range $0 < k_\mathrm{s} u_*/v < 5$ (Tani 1969; Schlichting 1979). The upper limit of this inequality determines the maximum value of the velocity at which laminar flow is possible. Taking into account that $u_* = \sqrt{\tau/\rho}$, $\tau = \mu(\mathrm{d}u/\mathrm{d}y)_\mathrm{w}$, $u = U_\mathrm{max}(1-\eta^2)$, $\eta = r/r_0$ and $U_\mathrm{max} = 2U$, where τ is the shearing stress at a wall, U_max and U are the maximum and average velocities, r_0 is the micro-channel radius, and subscript w refers to the wall, we arrive at the following estimate of the relative roughness, corresponding to the boundary that subdivides the laminar flow in smooth and rough channels, Hetsroni et al. (2005)

$$\frac{k_\mathrm{s}}{r_0} < \frac{5}{1.41\mathrm{Re}^{1/2}}\,. \tag{3.6}$$

For $\mathrm{Re} \sim 2 \times 10^3$, the relative roughness that corresponds to the boundary between the smooth and rough channels is $k_\mathrm{s}/r_0 \sim 0.08$. The latter shows that the hydraulic characteristics of the present micro-channels (Table 3.4) are close to characteristics of smooth micro-channels.

The deviation of the data related to flow in smooth (Table 3.3) and rough (Table 3.4) micro-channels may be a result of heterogeneity of the actual roughness, where height of some roughness peaks significantly exceeds its mean value. For example, under conditions of experiment by Pfund et al. (2000) the mean heigh of

Table 3.4 Experimental results of single-phase flow in rough micro-channels

Author	Micro-channel		Fluid	Re	Poiseuille number			Re_{cr}
	Shape	d_h [mm]			Po_{exp}/Po_{theor}	Dependence on Re	Relative roughness % $[k_s/r_0]$	
Peng, Peterson (1996)	Rectangular	133–367	Water	2×10^2–4×10^3	Inversely proport. to $Re^{0.98}$	Inversely proport. to $Re^{0.98}$		300–700
Peng, Wang (1998)	Rectangular	133–343	Water	2×10^2–4×10^3	Inversely proport. to $Re^{0.98}$	Inversely proport. to $Re^{0.98}$		300–700
Mala, Li (1999)	Circular tube	50–254	De-ion. water	10^2–2.1×10^3	1 for $Re < 500$	Independ. on Re at $Re < 500$	1.36–7	300–900
Qu et al. (2000)	Trapezoidal	51–169	De-ion. ultra filtered water	10^2–1.6×10^3	1.15–1.3	Weakly dependent on Re	3.6–5.7	1,000
Pfund et al. (2000)	Rectangular	Depth 257	De-ion. water	60–3,450	1.25	Independ. on Re at $Re < 1{,}700$	Mean 0.74 Max 5.7	1,700–2,000
Li et al. (2003)	Circular tube	128.76–179.8	De-ion. water	350–2,300	1.15–1.37	Weak depend. on Re at $Re < 1{,}500$	3–4	1,700
Kandlikar et al. (2003)	Circular tube	620–1,067	Water	500–2,600	~ 1	Independ. on Re at $Re < 2\times10^3$	0.32–0.71	$\sim 2{,}300$

the roughness wall was $\pm 1.9\,\mu m$, with the maximum peak value height of approximately $14.67\,\mu m$.

A study of forced convection characteristics in rectangular channels with hydraulic diameter of 133–367 μm was performed by Peng and Peterson (1996). In their experiments the liquid velocity varied from 0.2 to 12 m/s and the Reynolds number was in the range 50–4,000. The main results of this study (and subsequent works, e.g., Peng and Wang 1998) may be summarized as follows: (1) friction factors for laminar and turbulent flows are inversely proportional to $Re^{1.98}$ and $Re^{1.72}$, respectively; (2) the Poiseuille number is not constant, i.e., for laminar flow it depends on Re as $Po \sim Re^{-0.98}$; (3) the transition from laminar to turbulent flow occurs at Re about 300–700. These results do not agree with those reported by other investigators and are probably incorrect.

Mala and Li (1999) investigated experimentally the pressure losses in microchannels with diameters ranging from 50 to 254 μm. The micro-tubes were fabricated from two different materials, silica and stainless steel, and had mean surface roughness of $\pm 1.75\,\mu m$. Thus, the relative roughness changed from 1.36 to 7.0% for the pipes with $d = 254\,\mu m$ and $d = 50\,\mu m$, respectively. The measurements indicate the existence of significant divergence between experimental values of pressure gradient ΔP_{exp} and values predicted by the conventional theory, ΔP_{theor}. The difference $\Delta P_{exp} - \Delta P_{theor}$ depends on the diameter of the micro-tube, as well as on the Reynolds number. At relatively large Re the dependence $\Delta P(Re)$ is close to linear, whereas at $Re \sim 10^3$ and $d < 100\,\mu m$ it shows significant deviation from the dependence predicted by the Poiseuille equation. It is worth noting that there is some difference between pressure losses corresponding to flow in silica and stainless steel micro-tubes: the pressure gradient in a silica micro-tube is slightly higher than that for stainless steel. Under conditions corresponding to flow in micro-tubes with the same roughness, such a difference points to an existence of some non-hydrodynamic interaction between the fluid and micro-tube wall. Based on the dependence $C^* = f(Re)$, it is possible to select two branches corresponding to relatively low ($Re < 10^3$) and high ($Re > 10^3$) Reynolds numbers. Within the first branch the ratio is about of $C^* = 1.12$. At $Re > 10^3$ the ratio C^* increases with Re. The latter result means that within the ranges of Reynolds number of $0 < Re < 10^3$ and $10^3 < Re < 2 \times 10^3$ the friction factor is inversely proportional to Re and $(Re)^n$ ($n < 1$), respectively. Thus, the present results correspond (qualitatively) to the known data on the drag in macro-tubes at laminar and developed turbulent flows. The difference between the results corresponding to micro- and macro-rough tubes manifests itself as shift of the transition to low Reynolds number regions where $\lambda \sim 1/Re$ and $\lambda = const$. We suggest two possible reasons of the effects mentioned above: the first is an earlier transition from laminar to turbulent flow, and the second is the direct effect of roughness on the momentum changes in the liquid layer adjacent to the solid wall.

The hypothesis on the earlier transition from laminar to turbulent flow in micro-tubes is based on analysis of the dependence of pressure gradient on Reynolds number. As shown by the experimental data by Mala and Li (1999), this dependence may be approximated by three power functions: $\Delta P \sim Re^{1.072}$ ($Re < 600$),

$\Delta P \sim \mathrm{Re}^{1.3204}$ ($600 < \mathrm{Re} < 1{,}500$) and $\Delta P \sim \mathrm{Re}^{2.0167}$ ($1{,}500 < \mathrm{Re} < 2{,}200$) corresponding to laminar, transition and developed turbulent flow, respectively. Naturally, such phenomenological analysis does not reveal the actual reasons of the shift of the boundary transition to the low Reynolds numbers region.

One of the possible ways to account for the effect of roughness on the pressure drop in a micro-tube is to apply a modified-viscosity model to calculate the velocity distribution. Qu et al. (2000) performed an experimental study of the pressure drop in trapezoidal silicon micro-channels with the relative roughness and hydraulic diameter ranging from 3.5 to 5.7% and 51 to 169 μm, respectively. These experiments showed significant difference between experimental and theoretical pressure gradient.

It was found that the pressure gradient and flow friction in micro-channels were higher than that predicted by the conventional laminar flow theory. In a low Re range, the measured pressure gradient increased linearly with Re. For $\mathrm{Re} > 500$, the slope of the P_x–Re relationship increases with Re. The ratio C^* was about 1.3 for micro-channels of hydraulic diameter 51.3–64.9 μm and 1.15–1.18 for micro-channels of hydraulic diameter 114.5–168.9 μm. It was also found that the ratio of C^* depends on the Reynolds number.

A roughness-viscosity model was proposed to interpret the experimental data. An effective viscosity μ_{ef} was introduced for this purpose as the sum of physical μ and imaginary $\mu_M = \mu_M(r)$ viscosities. The momentum equation is

$$\frac{1}{r}\frac{\partial}{\partial r}\left(\mu_{\mathrm{ef}} r \frac{\partial u}{\partial r}\right) = \frac{\mathrm{d}P}{\mathrm{d}x} \tag{3.7}$$

with no-slip conditions on the walls, where μ_M is determined by a semi-empirical correlation $\mu_M = \mu f(r/k_\mathrm{s}, \mathrm{Re}, \mathrm{Re}_k)$, $\mathrm{Re}_k = u_k k_\mathrm{s}/\nu$, $\mathrm{Re} = Ud/\nu$, u_k is the velocity at the top of the roughness element, U is the average velocity, and d is the micro tube diameter. The correlation for μ_M also contains an empirical constant that has to be determined by using the experimental data.

Friction factors and the friction constant for a 257 μm deep channel with rough bottom plate were measured by Pfund et al. (2000). The width of the channel cut into each spacer was fixed at 1 cm. The micro-channel was 10 cm long, so that the flow profile would be fully developed within at least the middle third of the channel length. The wide channel gave an approximately 2D flow, thereby simplifying the theoretical description of the flow. Water entered the system through a pressured pulsation damper. The mean amplitude of roughness on the rough bottom was of ± 1.90 μm with a maximum peak-valley height of approximately 14.67 μm. The value of C^* reached, at low Re, approximately 1.25. These results were compared to those obtained in the smooth micro-channels with depths ranging from 128 to 521 μm. The authors conclude that a possible reduction in channel depth at constant roughness, and an increase in roughness at constant depth, produced no significant changes in the friction constant. Friction factors in laminar flow were proportional to $1/\mathrm{Re}$ to the degree of accuracy of the experiments. High relative roughness might cause the Poiseuille number to vary with Re. Uncertainties in the measured constant obscured this effect.

Li et al. (2003) studied the flow in a stainless steel micro-tube with the diameter of 128.76–179.8 μm and relative roughness of about 3–4%. The Poiseuille number for tubes with diameter 128.76 and 171.8 μm exceeded the value of Po corresponding to conventional theory by 37 and 15%, respectively. The critical value of the Reynolds number was close to 2,000 for 136.5 and 179.8 μm micro-tubes and about 1,700 for micro-tube with diameter 128.76 μm.

The effect of roughness on pressure drop in micro-tubes 620 and 1,067 μm in diameter, with relative roughness of 0.71, 0.58 and 0.321% was investigated by Kandlikar et al. (2003). For the 1,067 μm diameter tube, the effect of roughness on pressure drop was insignificant. For the 620 μm tube the pressure drop results showed dependence on the surface roughness.

3.4.3 Surfactant Solutions

Drag reduction in a surfactant solution flowing in a micro-channel was the subject of experimental study by Hetsroni et al. (2004). The pressure drop in fully developed laminar flow in a micro-tube of inner diameter 1.07 mm was measured in the range of $10 \leq \mathrm{Re} \leq 450$. The study was performed for water surfactant solution of 350 and 1,060 ppm in adiabatic and diabatic flows. The cationic surfactant Habon G (molecular weight 500, trade name Hoe S4089, Hoechst AG) was used. The cation of the surfactant is hexadecyldimethyl hydroxyethyl ammonium and the counter-ion is 3-hydroxy-z-naphthoate. It was shown by Zakin et al. (1996, 2002) that although micro-structure of Habon G was mechanically degraded under high-shear conditions, it recovered quickly, no matter how many times it was broken up by shear.

The measurements of physical properties were carried out over a wide range of temperatures and for various concentrations. All solutions were prepared by dissolving the powdered surfactant in de-ionized water with gentle stirring. The shear viscosity of all surfactant solutions was determined in the temperature range of 25 to 60 °C (Hetsroni et al. 2001). Figure 3.5 shows the effect of shear rate on shear viscosity for 1,060 ppm Habon G solutions at different temperatures. One can see that at low-shear rates, the shear viscosity of Habon G solution is significantly higher than that of clear water. The curves come closer to one another for higher shear rates. The magnitude of the shear viscosity as a function of the shear rate decreases when the temperature of the solution increases.

The plot of the pressure drop depending on the bulk velocity in adiabatic and diabatic flows is shown in Fig. 3.6a,b. The data related to the adiabatic flow correspond to constant temperature of the fluids $T_{\mathrm{in}} = 25\,^{\circ}\mathrm{C}$, whereas in the diabatic flow the fluid temperature increased along micro-channel approximately from 40 to 60 °C. It is seen that in both cases the pressure drop for Habon G increases compared to clear water. The difference between pressure drop corresponding to flows of a surfactant solution and solvent increases with increasing bulk velocity.

The experimental data on micro-channel drag are presented in Figs. 3.7 and 3.8 in the form of f versus Re where $f = (\Delta P d)/(2L\rho U^2)$, i.e., $f = \lambda/4$. The Reynolds

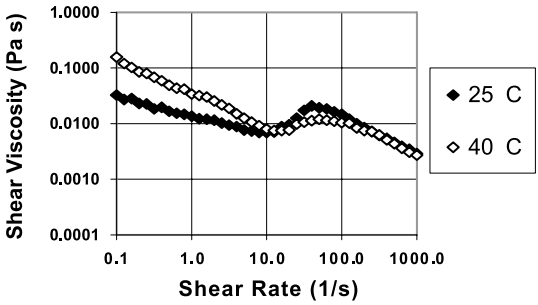

Fig. 3.5 Dependence of shear viscosity of Habon G solution on shear rate. Reprinted from Hetsroni et al. (2004) with permission

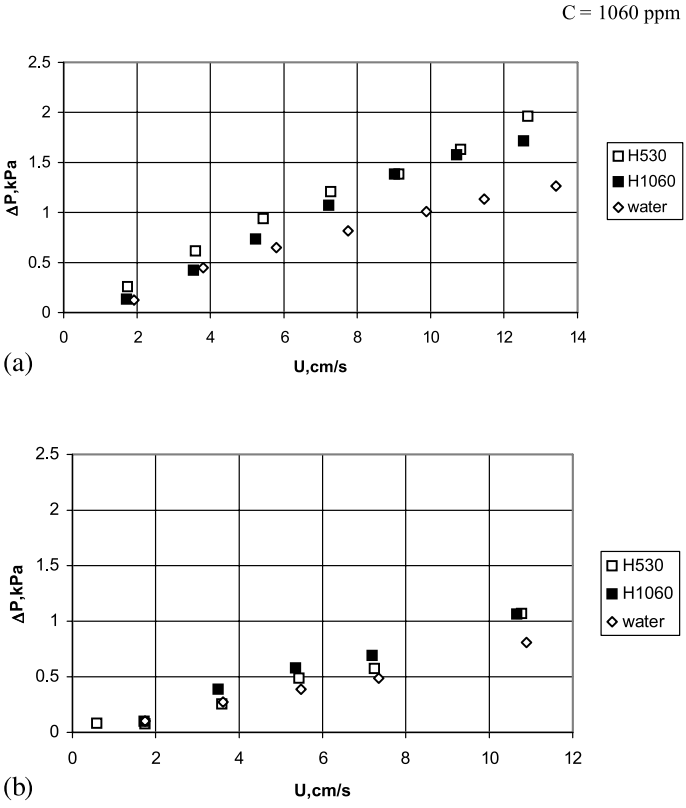

Fig. 3.6a,b Dependence of pressure drop on fluid bulk velocity in (**a**) adiabatic flow, and (**b**) diabatic flow. Reprinted from Hetsroni et al. (2004) with permission

numbers are defined based on the solvent ($\mathrm{Re_{wat}}$) or shear viscosity of Habon G ($\mathrm{Re_{sh}}$), where the shear viscosity, ν_{sh}, determines for a given value of shear rate that defined as $8U/d$ (Cogswell 1981). Figure 3.7a,b shows that the friction factor corresponding to the Habon G flow exceeds (at the same $\mathrm{Re_{wat}}$) the friction factor in the pure solvent flow. In contrast to that, the dependences for both 530 and 1,060 ppm Habon G solutions $f(\mathrm{Re_{sh}})$ are located significantly lower than that for a Newtonian

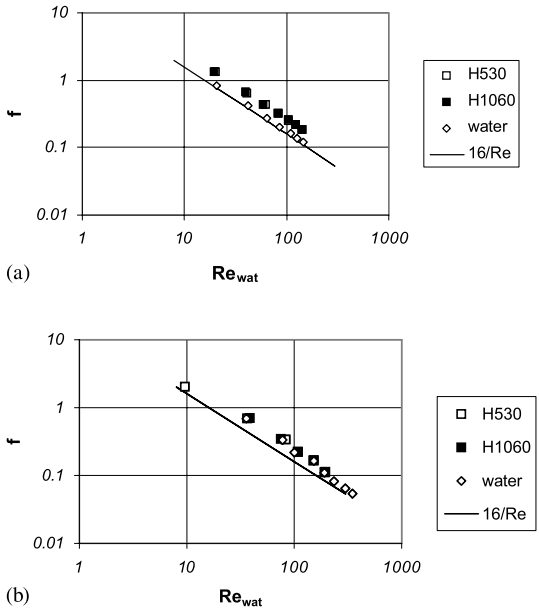

Fig. 3.7a,b Friction coefficients as function of solvent Reynolds number Re_{wat} in (**a**) adiabatic flow, and (**b**) diabatic flow. Reprinted from Hetsroni et al. (2004) with permission

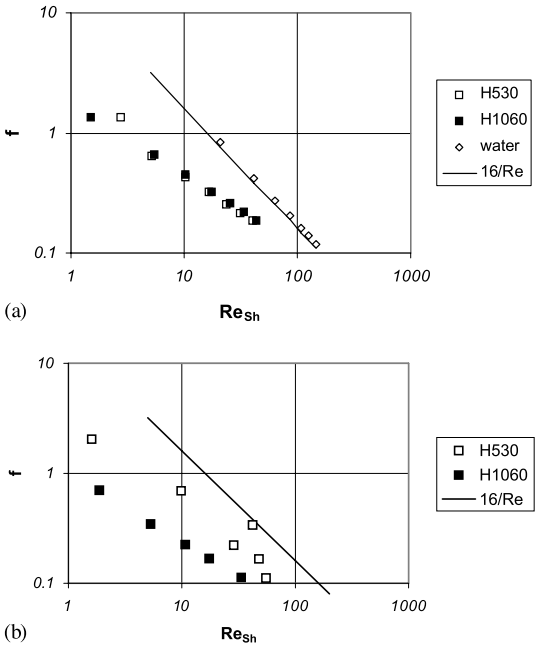

Fig. 3.8a,b Friction coefficients as a function of solution Reynolds number Re_{sh} in (**a**) adiabatic flow, and (**b**) diabatic flow. Reprinted from Hetsroni et al. (2004) with permission

fluid in a pipe with smooth walls, where the friction factor is $f = 16/\mathrm{Re}_{\mathrm{sh}}$. These results are somewhat unexpected. As can be concluded from Fig. 3.8a,b, the Habon G solutions are not drag reducing in laminar flow. The dependence of f versus $\mathrm{Re}_{\mathrm{sh}}$ does not reflect this phenomenon. The Reynolds number based on shear viscosity is not valid to describe drag reduction in laminar flow. According to Lumley (1969) definition the flows have to be compared using the same viscosity, given by the solution. It has become customary to use the kinematic viscosity of the solvent with respect to the definition of the friction factor as a function of the Reynolds number (Cho and Hartnett 1982; Zakin et al. 1996; Virk et al. 1970; Warholic et al. 1999).

3.5 Gas Flows

Gas flows are flows of compressible fluids that flow under conditions of gas expansion and changes its density, pressure, velocity and temperature along the channel length (Shapiro 1953). There is a paucity of theoretical study of laminar gas flows in micro-channels. Berg et al. (1993) considered this problem in conjunction with calculation of the viscosity from the data on mass flow rate. An experimental and theoretical investigation of low Reynolds number, high subsonic Mach number compressible gas flow in channels was presented by Harley et al. (1995). Nitrogen, helium, and argon gases were used. By means of analytical and numerical solutions of the problem the detailed data on velocity, density and temperature distributions along micro-channel's axis were obtained. The effect of the Mach number on profiles of axial and transverse velocities and temperature was revealed. The friction factor in trapezoidal micro-channels typically 100 μm wide, 10^4 μm long and ranging from 0.5 to 20 μm in depth, was measured. The measurements of the pressure drop for the flow of nitrogen, helium and argon were carried out by varying the Knudsen number from 10^{-3} to 0.4, the inlet and exit Mach numbers 0.07 and 0.15, and 0.22, and 0.84, respectively and $\mathrm{Re} < 2 \times 10^3$. Figure 3.9 shows that under conditions which correspond to continuum flow, the measured value of friction factor is close to that which is predicted by conventional theory: the average friction constant was within 3% of the theoretical value for fully developed incompressible flow.

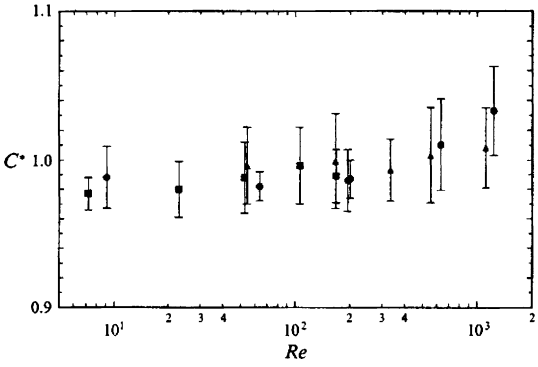

Fig. 3.9 Normalized Poiseuille number as a function of the Reynolds number in 11.04 μm deep channel. *Circles* (●) represent nitrogen, *squares* (■) represent helium, and *triangles* (▲) represent argon. Reprinted from Harley et al. (1995) with permission

3.6 Transition from Laminar to Turbulent Flow

The data on critical Reynolds numbers in micro-channels of circular and rectangular cross-section are presented in Tables 3.5 and 3.6, respectively. We also list geometrical characteristics of the micro-channels and the methods used for determination of the critical Reynolds number.

For the most part of the experiments one can conclude that transition from laminar to turbulent flow in smooth and rough circular micro-tubes occurs at Reynolds numbers about $\mathrm{Re_{cr}} = 2{,}000$, corresponding to those in macro-channels. Note that other results were also reported. According to Yang et al. (2003) $\mathrm{Re_{cr}}$ derived from the dependence of pressure drop on Reynolds number varied from $\mathrm{Re_{cr}} = 1{,}200$ to $\mathrm{Re_{cr}} = 3{,}800$. The lower value was obtained for the flow in a tube 4.01 mm in diameter, whereas the higher one was obtained for flow in a tube of 0.502 mm diameter. These results look highly questionable since they contradict the data related to the flow in tubes of diameter $d > 1$ mm. Actually, the 4.01 mm tube may be considered

Table 3.5 Critical Reynolds number in circular micro-channels

Author	Micro-channel				$\mathrm{Re_{cr}}$	Remarks: considered characteristic
	Smooth/ rough	d [μm]	L [mm]	L/d		
Li et al. (2003)	Smooth	79.9–449	14.56–118.9	182–714	2,000	Friction factor
Yang et al. (2003)	Smooth	502–4,010	200–1,000	244–567	2,200	Friction factor ($\mathrm{Re_{cr}} \sim 1200$–3800 – pressure gradient)
Maynes, Webb (2002)	Smooth	705	141.9	201.2	2,200	Friction factor
Mala, Li (1999)	Smooth	50–254	55–88		300–900	Pressure gradient
Li et al. (2003)	Rough	128–179.8	39.30–84.26	305–470	1,700–1,900	Friction factor
Kandlikar et al. (2003)	Rough	620–1,032	–	–	2,000	Friction factor
Sharp, Adrian (2004)	Smooth	50–247	–	–	1,800–2,200	Friction factor, centerline velocity, rms of centerline velocity fluctuations
Hwang, Kim (2006)	Smooth	244–792	400–462	583–1,639	$\sim 2{,}000$	Friction factor

Table 3.6 Critical Reynolds number in rectangular and trapezoidal micro-channels

Author	Micro-channel				Re_{cr}	Remarks: considered characteristic
	Smooth/ rough	H [μm]	L [mm]	L/H		
Xu et al. (2000)	Smooth	15.4	10–50	367–1,700	1,500	Friction factor
Pfund et al. (2000)	Smooth	128–1,050	100	95–781	1,700 for $H = 263$ μm 2,000–2,100 for $H = 521$ μm	Friction factor
Pfund et al. (2000)	Rough	257	100	389	1,700	Friction factor
Qu et al. (2000)	Rough (trapezoidal)	28–113.84	30	263–1,071	<2,300	Pressure gradient
Peng, Peterson (1996)	Rough	200–300	45	150–225	200–700	Friction factor

to be a macro-tube, in which the critical Reynolds number is about 2,000. A possible reason for this inconsistency arises from the method of determination of Re_{cr}. The data discussed above were obtained by analysis of the dependence of the pressure gradient on the Reynolds number. The same experimental data, presented by Yang et al. (2003) in the form of dependence of the friction factor on the Reynolds number, clearly showed that Re_{cr} is about 2,000. Mala and Li (1999), using the method based on dependence of the pressure drop gradient on Reynolds number, obtained $Re_{cr} = 300-900$.

The transition from laminar to turbulent flow in micro-channels with diameters ranging from 50 to 247 μm was studied by Sharp and Adrian (2004). The transition to turbulent flow was studied for liquids of different polarities in glass micro-tubes having diameters between 50 and 247 μm. The onset of transition occurred at the Reynolds number of about 1,800–2,000, as indicated by greater-than-laminar pressure drop and micro-PIV measurements of mean velocity and rms velocity fluctuations at the centerline.

In the laminar region the rms of streamwise velocity fluctuations was expected to be zero (Sharp et al. 2001). Figure 3.10 shows that the first evidence of transition, in the form of an abrupt increase in the rms, occurs at $1{,}800 \leq Re \leq 2{,}200$, in full agreement with the flow resistance data. There was no evidence of transition below these values. Thus, the behavior of the flow in micro-tubes, at least down to a 50 μm diameter, shows no perceptible differences with the macro-scale flow.

Hwang and Kim (2006) investigated the pressure drop in circular stainless steel smooth micro-tubes ($k_s/d < 0.1\%$) with inner diameters of 244 μm, 430 μm and 792 μm. The measurements showed that the onset of flow transition from laminar to turbulent motion occurs at the Reynolds number of slightly less than 2,000. It

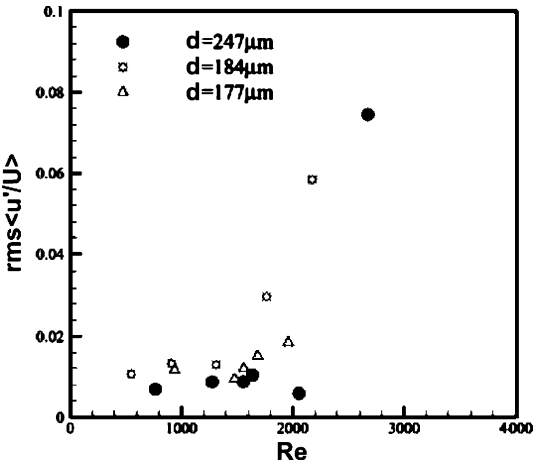

Fig. 3.10 Measured rms of the centerline velocity, divided by measured average velocity, vs. the Reynolds number. Reprinted from Sharp et al. (2001) with permission

also showed that the conventional theory predicted the friction factor well within an absolute average deviation of 8.9%.

Hao et al. (2007) investigated the water flow in a glass tube with diameter of 230 μm using micro particle velocimetry. The streamwise and mean velocity profile and turbulence intensities were measured at Reynolds number ranging from 1,540 to 2,960. Experimental results indicate that the transition from laminar to turbulent flow occurs at Re = 1,700−1,900 and the turbulence becomes fully developed at Re > 2,500.

Thus, the available data related to transition in circular micro-tubes testify to the fact that the critical Reynolds number, which corresponds to the onset of such transition, is about 2,000. The evaluation of critical Reynolds number in irregular micro-channels will entail great difficulty since this problem contains a number of characteristic length scales. This fact leads to some vagueness in definition of critical Reynolds number that is not a single criterion, which determines flow characteristics.

Let us explain this assertion by an example of the developed laminar flow in a rectangular micro-channel. As is well known (Loitsianskii 1966) this problem reduces to integrating the momentum equation

$$\mu\left(\frac{\partial^2 u}{\partial y^2}+\frac{\partial^2 u}{\partial z^2}\right)=\frac{\mathrm{d}P}{\mathrm{d}x}=-\frac{\Delta P}{L} \tag{3.8}$$

with the following boundary conditions

$$u=0 \text{ at } y=\pm H,\ |z|<W; u=0 \text{ at } z=\pm W,\ |y|<H \tag{3.9}$$

where u is the longitudinal velocity component, $\Delta P/L$ is the pressure drop per unit length, μ is dynamic viscosity, and $2H$ and $2W$ are the depth and width of the micro-channel.

Bearing in mind the conditions of the problem, we can assume that pressure drop per unit length is determined by viscosity, average velocity, as well as the depth and width of the micro-channel:

$$\frac{\Delta P}{L} = f(\mu, U, H, W) \tag{3.10}$$

where U is the average velocity.

Applying the Π-theorem to Eq. (3.10), we arrive at the following expression for the friction factor

$$\lambda = \frac{\varphi(\varepsilon)}{\mathrm{Re}_*} \tag{3.11}$$

where $\mathrm{Re}_* = U2H/\nu$ is the Reynolds number determined by micro-channel depth, λ is the friction factor, $\varphi(\varepsilon)$ is some unknown function of channel aspect ratio, $\varepsilon = W/H$, and ν is the kinematic viscosity of fluid.

It appears that the Poiseuille number in a rectangular channel depends on the aspect ratio, ε. In order to reveal an explicit form of the dependence $\varphi(\varepsilon)$, it is necessary to solve the problem defined by Eqs. (3.8) and (3.9) to obtain

$$\varphi(\varepsilon) = \frac{128}{\psi(\varepsilon)} \tag{3.12}$$

where $\psi(\varepsilon) = \frac{16}{3} - \frac{1024}{\pi^5 \varepsilon}(th\frac{\pi\varepsilon}{2} + \frac{1}{3^3}th\frac{3\pi\varepsilon}{2} + \ldots)$.

Equations (3.11) and (3.12) show that the friction factor of a rectangular micro-channel is determined by two dimensionless groups: (1) the Reynolds number that is defined by channel depth, and (2) the channel aspect ratio. It is essential that the introduction of a hydraulic diameter as the characteristic length scale does not allow for the reduction of the number of dimensionless groups to one. We obtain

$$\lambda = \frac{\varphi'(\varepsilon)}{\mathrm{Re}_\mathrm{h}} \tag{3.13}$$

where $\varphi'(\varepsilon) = (\varphi(\varepsilon)2\varepsilon)/(1+\varepsilon)$. Accordingly, the Poiseuille number that is defined by hydraulic diameter depends also on channel aspect ratio.

The results related to the laminar-to-turbulent transition can be generalized by using the Obot–Jones model (Jones 1976; Obot 1988). A detailed discussion of this model is found in the paper by Morini (2004).

An experimental study of the laminar-turbulent transition in water flow in long circular micro-tubes, with diameter and length in the range of 16.6–32.2 μm and 1–30 mm, respectively, was carried out by Rands et al. (2006). The measurements allowed to estimate the effect of heat released by energy dissipation on fluid viscosity under conditions of laminar and turbulent flow in long micro-tubes.

The data on the drag for micro-tube diameters of 16.6, 19.7, 26.3 and 32.2 μm are presented in Fig. 3.11 in the form of the dependence of the Poiseuille number on Re. The latter was determined by an average of the mixed-mean temperature at the inlet and outlet of the micro-tube. The data of Fig. 3.11 show that the Poiseuille number practically shows no dependence on Re in the range $500 < \mathrm{Re} < 2{,}000$. The

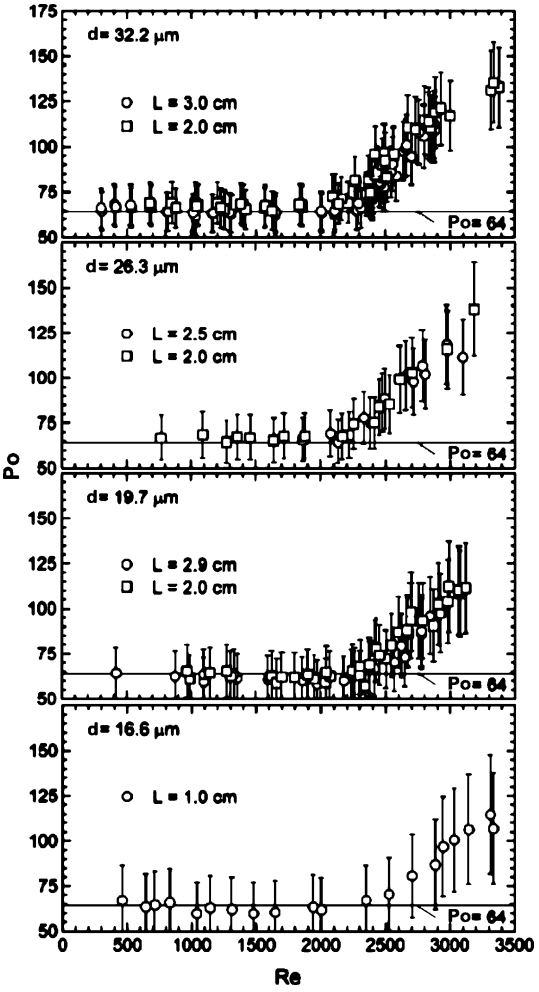

Fig. 3.11 Dependence of the Poiseuille number on Reynolds number. Reprinted from Rands et al. (2006) with permission

absolute of Po is close to 64, corresponding to the predictions of the conventional theory. The transition from laminar to turbulent flow occurs at Re = 2,100−2,500.

The dependence of the measured rise in fluid mixed-cup temperature on Reynolds number is illustrated in Fig. 3.12. The difference between outlet and inlet temperatures increases monotonically with increasing Re at laminar and turbulent flows. Under conditions of the given experiments, the temperature rise due to energy dissipation is very significant: $\Delta T = 15-35$ K at $L/d = 900-1{,}470$ and Re = 2,500. The data on rising temperature in long micro-tubes can be presented in the form of the dependence of dimensionless viscous heating parameter $\mathrm{Re}/[\mathrm{Ec}(L/d)]$ on Reynolds number (Fig. 3.13).

In the latter figure, the theoretical dependence

$$\mathrm{Re}/[\mathrm{Ec}(L/d)] = 32 \tag{3.14}$$

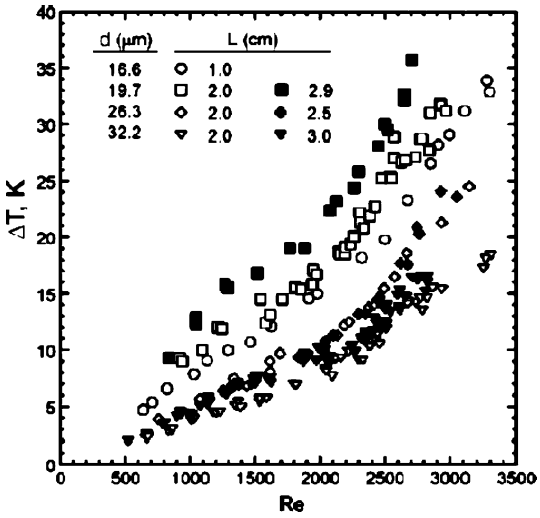

Fig. 3.12 Increase in the fluid average temperature. Reprinted from Rands et al. (2006) with permission

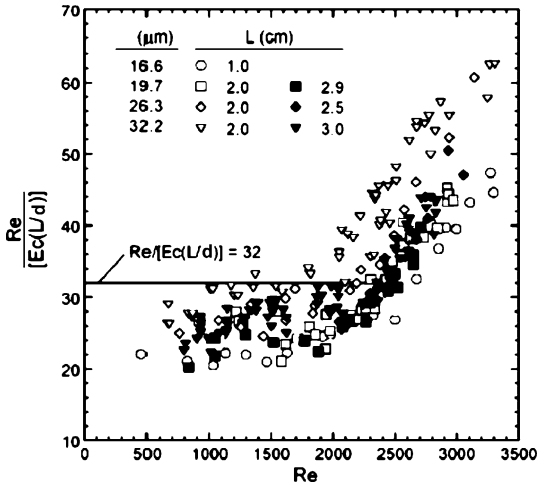

Fig. 3.13 Variation of the viscous heating parameter $\mathrm{Re}/[\mathrm{Ec}(L/d)]$ with Reynolds number. Reprinted from Rands et al. (2006) with permission

corresponding to laminar flow in an adiabatic micro-tube is also presented. It is seen that at relatively low Reynolds numbers that correspond to laminar flow, the viscous heating parameter does not depend on Re. At $\mathrm{Re} > 2{,}000$ the shape of the dependence $\mathrm{Re}/[\mathrm{Ec}(L/d)] = f(\mathrm{Re})$ sharply changes. An increase in the Reynolds number leads to an increase in the viscous heating parameter. Thus, both characteristic parameters of flow Po and $\mathrm{Re}/[\mathrm{Ec}(L/d)]$ that account for the hydraulic resistance and energy dissipation change identically with the Reynolds number. In the range of relatively low Reynolds numbers, $\mathrm{Re} < 2{,}000$, they are constant, whereas at $\mathrm{Re} > 2{,}000-2{,}500$ the Poiseuille number and viscous heating parameter monotonically increase with increasing Re. The latter testifies to the fundamental transformation of the flow structure, which occurs in this range of Re, and the Reynolds

numbers in the range of 2,000–2,500 can be considered as critical corresponding to the transition from laminar to turbulent flow in micro-tubes.

3.7 Effect of Measurement Accuracy

In experiments related to flow and heat transfer in micro-channels, some parameters, such as the flow rate and channel dimensions are difficult to measure accurately because they are very small. For a single-phase flow in micro-channels the uncertainty of $\lambda \mathrm{Re}$ is (Guo and Li 2002, 2003)

$$\frac{\delta(\lambda \mathrm{Re})}{\lambda \mathrm{Re}} = \left\{ \left(\frac{\delta(\Delta P)}{\Delta P} \right)^2 + \left(\frac{4(\delta d_\mathrm{h})}{d_\mathrm{h}} \right)^2 + \left(\frac{\delta(L)}{L} \right)^2 + \left(\frac{\delta(m)}{m} \right)^2 \right\}^{1/2} \tag{3.15}$$

where m, ΔP, d_h, L are the mass flow rate, pressure drop, hydraulic diameter and channel length, respectively. Equation (3.15) shows that the channel hydraulic diameter measurement error may play a very important part in the resulting uncertainty of the product $\lambda \mathrm{Re}$. For example, in experiments measuring the friction factor in a circular glass micro-tube by Guo and Li (2002), they initially measured the diameter as 84.7 μm using a 40× microscope. The data reduction with this diameter showed that the friction factors were larger than that predicted by the conventional theory. The averaged value of the diameter measured using a 400× microscope and scanning electron microscope for the same micro-tube was only 80.0 μm. With this more accurate value of the diameter, the friction factors obtained from the experimental data were in good agreement with the conventional values.

3.8 Specific Features of Flow in Micro-Channels

3.8.1 General Remarks

The data presented in the previous chapters, as well as the data from investigations of single-phase forced convection heat transfer in micro-channels (e.g., Bailey et al. 1995; Guo and Li 2002, 2003; Celata et al. 2004) show that there exist a number of principal problems related to micro-channel flows. Among them there are: (1) the dependence of pressure drop on Reynolds number, (2) value of the Poiseuille number and its consistency with prediction of conventional theory, and (3) the value of the critical Reynolds number and its dependence on roughness, fluid properties, etc.

All available experimental data (except the data by Peng and Peterson 1996; Peng and Wang 1998) show that the friction factor is inversely proportional to the Reynolds number, i.e., $\lambda = \mathrm{const}/\mathrm{Re}$. The constant depends on the micro-channel shape only and agrees fairly well with the result of a dimensional analysis carried

out by Sedov (1993) and the analytical solution of the problem (Loitsianskii 1966). The qualitative difference between the data by Peng and Peterson (1996) and Peng and Wang (1998) and the experimental and theoretical data of other researchers is, probably, due to experimental uncertainties.

Concerning the critical Reynolds number, several groups of experiments related to laminar-to-turbulent flow can be set apart (Tables 3.5 and 3.6):

- Li et al. (2003), Yang et al. (2003), Maynes and Webb (2002), Kandlikar et al. (2003) and Sharp and Adrian (2004) obtained the critical Reynolds number in the range $\mathrm{Re_{cr}} \approx 1{,}700-2{,}300$.
- Li et al. (2003), Xu et al. (2000), and Pfund et al. (2000) also obtained the critical Reynolds number $\mathrm{Re_{cr}} \approx 1{,}500-1{,}900$.
- Peng and Peterson (1996), Peng and Wang (1998), and Mala and Li (1999) obtained the anomalously low critical Reynolds number $\mathrm{Re_{cr}} \approx 200-900$.

The critical Reynolds numbers of 1,700–2,300 agree fairly well with the well-known values of $\mathrm{Re_{cr}}$ corresponding to flow in macro-channels (Lindgren 1958; Leite 1959; Wygnanskii and Champagne 1973; Schlichting 1979). This result is not unexpected since from a simple physical consideration it is obvious that under conditions of the continuous model with viscous fluid/wall interaction and moderate flow velocity, when energy dissipation is negligible, there are no reasons for a decrease in the critical Reynolds number. Taking into consideration the dimension of the characteristic parameters, we determine in this case that the lifetime of vortices is inversely proportional to the fluid viscosity

$$t \sim \frac{d^2}{\nu}. \tag{3.16}$$

The characteristic hydrodynamic time, t_h is

$$t_\mathrm{h} = \frac{L}{U} \tag{3.17}$$

and

$$\frac{t}{t_\mathrm{h}} \sim \frac{\mathrm{Re}}{\overline{L}} \tag{3.18}$$

where $\overline{L} = L/d$.

The ratio of t/t_h, which is characteristic of the possibility of vortices, does not depend on the micro-channel diameter and is fully determined by the Reynolds number and L/d. The lower value of Re at which $t/t_\mathrm{h} \geq 1$ can be treated as a threshold. As was shown by Darbyshire and Mullin (1995), under conditions of an artificial disturbance of pipe flow, a transition from laminar to turbulent flow is not possible for $\mathrm{Re} < 1{,}700$, even with a very large amplitude of disturbances.

A direct study of the transition from laminar to turbulent flow in micro-tubes was performed by Sharp and Adrian (2004). The measurements of mean velocity and rms of velocity fluctuations showed that the value of the Reynolds number, at which the transition from laminar to turbulent flow occurs, is about $\mathrm{Re_{cr}} \approx 1{,}800-2{,}200$.

Thus, the measurements of integral flow characteristics, as well as mean velocity and rms of velocity fluctuations testify to the fact that the critical Reynolds number is the same as Re_{cr} in the "macroscopic" Poiseuille flow. Some decrease in the critical Reynolds number down to $Re \sim 1{,}500-1{,}700$, reported by the second group above, may be due to energy dissipation. The energy dissipation leads to an increase in fluid temperature. As a result, the viscosity would increase in gas and decrease in liquid. Accordingly, in both cases the Reynolds number based on the inlet flow viscosity differs from that based on local viscosity at a given point in the micro-channel.

There is a significant scatter between the values of the Poiseuille number in micro-channel flows of fluids with different physical properties. The results presented in Table 3.1 for de-ionized water flow, in smooth micro-channels, are very close to the values predicted by the conventional theory. Significant discrepancy between the theory and experiment was observed in the cases when fluid with unknown physical properties was used (tap water, etc.). If the liquid contains even a very small amount of ions, the electrostatic charges on the solid surface will attract the counter-ions in the liquid to establish an electric field. Fluid-surface interaction can be put forward as an explanation of the Poiseuille number increase by the fluid ionic coupling with the surface (Brutin and Tadrist 2003; Ren et al. 2001; Papautsky et al. 1999).

The results obtained by Brutin and Tadrist (2003) showed a clear effect of the fluid on the Poiseuille number. Figure 3.14 shows results of experiments that were done in the same experimental set-up for hydraulic diameters of 152 and 262 μm, using distilled water and tap water. The ion interactions with the surface can perhaps explain such differences. Tap water contains more ions such as Ca^{2+}, Mg^{2+}, which are 100 to 1,000 times more concentrated than H_3O^+ or OH^-. In distilled water only H_3O^+ and OH^- exist in equal low concentrations. The anion and cation interactions with the polarized surface could modify the friction factor. This is valid only in the case of a non-conducting surface.

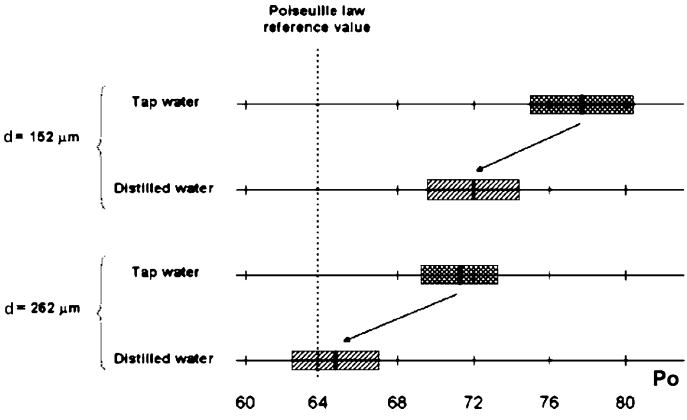

Fig. 3.14 Effect of the fluid on Poiseuille number. Reprinted from Brutin and Tadrist (2003) with permission

3.8.2 Thermal Effects

Gruntfest et al. (1964) showed that the thermal effects due to energy dissipation of liquid flow in a pipe lead to significant transformation of the flow field. It occurs due to the dependence of liquid density on temperature, distortion of velocity profile and development of flow instability and its transition to turbulence. The influence of energy dissipation on thermo- and hydrodynamic characteristics of the liquid flow in micro-channels was considered by Tso and Mahulikar (1998, 1999, 2000). A detailed analysis of viscous dissipation effects in micro-tubes and micro-channels was performed by Koo and Kleinstreuer (2004). It was shown that viscous dissipation becomes significant for fluids with low specific heat capacities and high viscosities, even in relatively low Reynolds number flows. The channel size, aspect ratio of the channel diameter to its length, as well as the Reynolds and Brinkman numbers are important factors that determine the effect of viscous dissipation.

Celata et al. (2005) evaluated the effect of viscous heating on friction factor for flow of an incompressible fluid in a micro-channel. By integrating the energy equation over the micro-channel length, a criterion that determines conditions when viscous dissipation effect is significant was obtained:

$$\frac{\mathrm{Ec}}{\mathrm{Re}}\left(\lambda \mathrm{Re}\overline{L}\right) \geq 1\,. \tag{3.19}$$

The simplest evaluation value of the complex $(\mathrm{Ec}/\mathrm{Re})\left(\lambda \mathrm{Re}\overline{L}\right)$ shows that it is essentially smaller than unity for the realistic conditions typical for water flow in micro-channels: $\mathrm{Re} \sim 10^3$, $d_\mathrm{h} \sim 100\,\mu\mathrm{m}$, $\overline{L} \sim 500$.

The behavior of liquid flow in micro-tubes and channels depends not only on the absolute value of the viscosity but also on its dependence on temperature. The nonlinear character of this dependence is a source of an important phenomenon – hydrodynamic thermal explosion, which is a sharp change of flow parameters at small temperature disturbances due to viscous dissipation. This is accompanied by radical changes of flow characteristics. Bastanjian et al. (1965) showed that under certain conditions the steady-state flow cannot exist, and an oscillatory regime begins.

We can estimate the effect of energy dissipation on liquid heating and values of flow parameters corresponding to arising oscillations in the flow. We assume that the density of the fluid and its thermal conductivity are constant. Then, the energy equation attains the form

$$\rho(v\nabla)h = k\nabla^2 T + \Phi \tag{3.20}$$

where h is the enthalpy, k is the thermal conductivity, and Φ is the energy dissipation. The present analysis is restricted to estimation of the maximum heating of the liquid that corresponds to adiabatic flow in a micro-channel.

For laminar flow

$$u = U_\mathrm{max}(1-\eta^2) \tag{3.21}$$

where $U_\mathrm{max} = 2U$ or $U_\mathrm{max} = 3U/2$ for axisymmetric and plane flows, respectively. Hence, we obtain from Eq. (3.20) the following estimation for adiabatic rise of the

liquid temperature:

$$\frac{\Delta T}{T_{\text{in}}} = 2\frac{\nu^2}{r_0^2}\left(\frac{L}{r_0}\right)\frac{\text{Re}}{c_{\text{p}}T_{\text{in}}} \tag{3.22}$$

for circular micro-channel, and

$$\frac{\Delta T}{T_{\text{in}}} = 12\frac{\nu^2 L\text{Re}}{H^2 d_{\text{h}} c_{\text{p}} T_{\text{in}}} \tag{3.23}$$

for plane micro-channel, where $\Delta T = T_{\text{out}} - T_{\text{in}}$ is the difference between outlet and inlet temperatures. The difference between outlet and inlet temperatures essentially depends on the heat capacity of the fluid and sharply increases as c_{p} decreases.

Estimation of adiabatic increase in the liquid temperature in circular micro-tubes with diameter ranging from 15 to 150 μm, under the experimental conditions reported by Judy et al. (2002), are presented in Table 3.7. The calculations were carried out for water, isopropanol and methanol flows, respectively, at initial temperature $T_{\text{in}} = 298$ K and $\nu = 8.7\times10^{-7}\,\text{m}^2/\text{s}$, $2.5\times10^{-6}\,\text{m}^2/\text{s}$, $1.63\times10^{-6}\,\text{m}^2/\text{s}$, and $c_{\text{p}} = 4{,}178\,\text{J/kg K}$, $2{,}606\,\text{J/kg K}$, $2{,}531\,\text{J/kg K}$, respectively. The lower and higher values of $\Delta T/T_{\text{in}}$ correspond to limiting values of micro-channel length and Reynolds numbers. Table 3.7 shows adiabatic heating of liquid in micro-tubes can reach ten degrees: the increase in mean fluid temperature $(T_{\text{in}}+T_{\text{out}})/2$ is about 9 °C, 121 °C, 38 °C for the water ($d = 20\,\mu$m), isopropanol ($d = 20\,\mu$m) and methanol ($d = 30\,\mu$m) flows, respectively.

Energy dissipation also significantly affects the temperature of gas flow. In order to estimate adiabatic increase in gas temperature in micro-channels we used the approximate expression for $\Delta T/T_{\text{in}}$, which follows from Eq. (3.23) assuming that $k\nabla^2 T \sim 0$, $h = c_{\text{p}}T$, $\Phi = \mu\left(\frac{\text{d}u}{\text{d}y}\right)^2 \sim \mu\frac{U^2}{\delta^2}$ and $\frac{\text{d}T}{\text{d}x} = \frac{T_{\text{out}}-T_{\text{in}}}{L}$:

$$\frac{\Delta T}{T_{\text{in}}} = \frac{\nu^2}{2\delta^2 c_{\text{p}} T_{\text{in}}}\left(\frac{L}{\delta}\right)\text{Re} \tag{3.24}$$

where $\delta = d_{\text{h}}/2$ and U are characteristic size and average velocity, $\text{Re} = U2\delta/\nu$.

Table 3.7 Estimation of adiabatic increase in the liquid temperature in a circular micro-tube. Experimental conditions correspond to those of Judy et al. (2002)

d [μm]	L [m]	Re	$(\Delta T/T_{\text{in}})\cdot 10^2$		
			Water	Isopropanol	Methanol
15	0.036	34–41	0.35–0.43	4.7–5.6	2.0–2.5
20	0.03–0.05	18–989	0.066–6.0	0.87–80	0.38–35
30	0.04–0.07	8–1,716	0.012–4.3	0.15–57	0.067–25
40	0.05–0.37	17–769	0.013–4.3	0.17–57	0.075–25
50	0.07–0.29	44–1,451	0.024–3.3	0.32–43	0.14–19
75	0.3–0.39	146–1,883	0.10–1.7	1.3–22	0.59–9.8
100	0.39	109–1,858	0.041–0.70	0.55–9.3	0.24–4.1
150	0.2–0.3	137–1,540	0.0079–0.13	0.11–1.8	0.046–0.77

For parameters presented in Table 3.8, which correspond to conditions in the experiments by Harley et al. (1995), the mean increase in the temperature of nitrogen, helium and argon ($\mathrm{Re}_{\mathrm{N}_2} = 60$, $\mathrm{Re}_{\mathrm{He}} = 20$, $\mathrm{Re}_{\mathrm{Ar}} = 50$, $T_{\mathrm{in}} = 300\,\mathrm{K}$, $M \sim 0.1$) is about 50–200 K (Table 3.9).

Energy dissipation leads to a significant increase in gas viscosity and decrease in the actual Reynolds number $\mathrm{Re}_{\mathrm{ac}}$ defined by the mean viscosity $\nu_{\mathrm{ac}} = (\nu_{\mathrm{out}} + \nu_{\mathrm{in}})/2$ compared to that defined by inlet parameters.

Under conditions of real experiments, the thermal regime of the flow determines not only the energy dissipation, but also the heat losses to the micro-channel walls. In this case increase in the fluid temperature depends on the relation between the rate of heat release by energy dissipation and heat losses due to heat transfer (Koo and Kleinstreuer 2004). This does not distort the qualitative picture of the phenomenon – in all cases energy dissipation leads to temperature growth, changing viscosity of fluid and actual Reynolds number. Moreover, in certain cases, energy dissipation leads to radical transformation of flow and transition from a stable to an oscillatory regime.

3.8.3 Oscillatory Regimes

To estimate the parameters resulting in such transitions we use the approach by Bastanjian et al. (1965) and Zel'dovich et al. (1985). The momentum and energy equations for a steady and fully developed flow in a circular tube are

$$\frac{1}{r}\frac{\partial}{\partial r}\left(r\mu\frac{\partial u}{\partial r}\right) - \frac{\mathrm{d}P}{\mathrm{d}x} = 0 \tag{3.25}$$

$$\frac{\partial^2 T}{\partial r^2} + \frac{1}{2}\frac{\partial T}{\partial r} + \frac{\mu}{kT}\left(\frac{\partial u}{\partial r}\right)^2 = 0 \tag{3.26}$$

Table 3.8 Characteristics of a micro-channel in the experiments by Harley et al. (1995)

Top width [μm]	Bottom width [μm]	Depth [mm]	Hydraulic diameter d_{h} [μm]	Length L [mm]	L/d_{h}	Gases tested
94.4	80.0	11.04	19.18	10.18	992.1	N_2, He, Ar

Table 3.9 Estimation of adiabatic increase in average gas temperature in experiments by Harley et al. (1995)

Gases	$\Delta T/T_{\mathrm{in}}$	$\Delta T_{\mathrm{av}}/T_{\mathrm{in}}$	$\nu_{\mathrm{ac}}/\nu_{\mathrm{in}}$	$R_{\mathrm{ac}}/R_{\mathrm{in}}$
Nitrogen	0.37	0.18	~1.35	~0.74
Helium	1.522	0.761	~2.87	~0.35
Argon	0.096	0.048	~1.09	~0.919

where $\mu = \mu(T)$.

The dependence of the liquid viscosity on the temperature is given by Frenkel (1946):

$$\mu = \mu_0 \exp\left(\frac{E}{RT}\right). \tag{3.27}$$

Using the Frank-Kamenetskii (1969) transformation we present the relation in Eq. (3.27) in the following form (Zel'dovich et al. 1985):

$$\mu = \mu_0 \exp\left(\frac{E}{RT_0}\right) \exp\left(-\frac{E(T-T_0)}{RT_0^2}\right) \tag{3.28}$$

where E is activation energy, R is the universal gas constant, $\mu_0 = f(T_0)$, T_0 is the characteristic temperature.

Introducing new variables

$$\xi = \left(\frac{r}{r_0}\right)^2, \quad \theta = \frac{E(T-T_0)}{RT_0^2} \tag{3.29}$$

we reduce the energy equation (3.20) to the following form (Zel'dovich et al. 1985):

$$\frac{\partial^2\theta}{\partial\xi^2} + \frac{1}{\xi}\frac{\partial\theta}{\partial\xi} + \chi\,\mathrm{e}^{\theta} = 0 \tag{3.30}$$

where the dimensionless parameter χ is

$$\chi = \frac{(\partial_x P)^2 r_0^4}{16\mu_0 k}\frac{E}{RT_0^2}\exp\left(-\frac{E}{RT_0}\right). \tag{3.31}$$

The boundary conditions corresponding to constant temperature are

$$\theta(1) = 0, \quad \left(\frac{\partial\theta}{\partial\xi}\right)_{\xi=0} = 0. \tag{3.32}$$

A steady-state solution of Eq. (3.30) exists only for $\chi \le 2$. At $\chi > 2$ hydrodynamic thermal explosion occurs and oscillatory flow takes place.

Bearing in mind that $\Delta P = \lambda\frac{L}{d}\frac{\rho U^2}{2}$, $\lambda = \frac{64}{\mathrm{Re}}$, $U = \frac{\mathrm{Re}\nu}{d}$, $\partial_x P = \frac{\Delta P}{L} = 32\frac{\rho\nu^2}{d^3}\mathrm{Re}$, and assuming that $\frac{\mu_0}{\rho} \simeq \nu_0 \approx \nu$ we obtain

$$\chi = \frac{\mathrm{Re}^2}{r_0^2}\frac{\nu_0^2}{c_\mathrm{p}T_0}\frac{E}{RT_0}\exp\left(-\frac{E}{RT_0}\right)\mathrm{Pr} \tag{3.33}$$

or

$$\mathrm{Re}_\mathrm{cr} = \left(\frac{\chi_\mathrm{cr}}{N}\right)^{1/2} r_0 \tag{3.34}$$

where $\chi_\mathrm{cr} = 2$, $N = \mathrm{Pr}\frac{\nu_o^2}{C_p T_0}\frac{E}{RT_0}\exp\left(-\frac{E}{RT_0}\right)$.

From approximation of actual values $\mu(T)$ and E/R in the range of $T = 273-323$ K it was found $E/R = 2{,}090$ K and $\mu_0 = 0.845 \times 10^{-6} Pas$ at $T_0 = 300$ K.

We estimate the critical Reynolds number for flows of water and transformer oil, using the physical properties presented by Vargaftik et al. (1996) to be

$$\mathrm{Re}_{\mathrm{cr}} = 1.94 \times 10^{10} r_0 \tag{3.35}$$

for water, and

$$\mathrm{Re}_{\mathrm{cr}} = 2.5 \times 10^{8} r_0 \tag{3.36}$$

for transformer oil, where r_0 is the micro-channel radius in meters.

The critical Reynolds number depends significantly on physical properties of the liquid (kinematic viscosity, heat capacity and the Prandtl number), and micro-channel radius. For flow of highly viscous liquids, e.g., transformer oil, in micro-channels of $r_0 < 10^{-5}$ m, the critical Reynolds number is less than 2,300. Under these conditions, oscillatory regime occurs at all Re corresponding to laminar flow. The existence of velocity fluctuations does not indicate a change of the flow regime from laminar to turbulent. This phenomenon shows only the occurrence of oscillatory laminar flow. In water flow (small kinematic viscosity, large heat capacity) rising of velocity oscillations is not possible at any realistic r_0.

Thus, the comparison of experimental results to those obtained by conventional theory is correct when the experimental conditions were consistent with the theoretical ones. The experimental results corresponding to these requirements agree quite well with the theory:

- For single-phase fluid flow in smooth micro-channels of hydraulic diameter from 15 to 4,010 μm, in the range of the Reynolds numbers $\mathrm{Re} < \mathrm{Re}_{\mathrm{cr}}$, the Poiseuille number, Po, is independent of the Reynolds number, Re.
- For single-phase gas flow in micro-channels of hydraulic diameter from 101 to 4,010 μm, in the range of Reynolds numbers $\mathrm{Re} < \mathrm{Re}_{\mathrm{cr}}$, the Knudsen number $0.001 \leq \mathrm{Kn} \leq 0.38$, and the Mach number $0.07 \leq \mathrm{Ma} \leq 0.84$, the experimental friction factor agrees quite well with the theoretical one predicted for fully developed laminar flow.
- The behavior of the flow in micro-channels, at least down to 50 μm in diameter, shows no difference with macro-scale flow. For smooth and rough micro-channels with relative roughness $0.32\% \leq k_{\mathrm{s}} \leq 7\%$, the transition from laminar to turbulent flow occurs between $1{,}800 \leq \mathrm{Re}_{\mathrm{cr}} \leq 2{,}200$, in full agreement with flow visualization and flow resistance data. In the articles used for the present study there was no evidence of transition below these results.
- The relation of hydraulic diameter to channel length and the Reynolds number are important factors that determine the effect of the viscous energy dissipation on flow parameters.
- Under certain conditions the energy dissipation may lead to an oscillatory regime of laminar flow in micro-channels. The oscillatory flow regime occurs in micro-channels at Reynolds numbers less that $\mathrm{Re}_{\mathrm{cr}}$. In this case the existence of velocity fluctuations does not indicate change from laminar to turbulent flow.

3.8.4 Laminar Drag Reduction in Micro-Channels Using Ultrahydrophobic Surfaces

The question of the conditions to be satisfied by a moving fluid in contact with a solid body was one of considerable difficulty for quite some time, as pointed out by Goldstein (1965), and the assumption of no-slip is now generally accepted for practical purposes. On the other hand, if we can make an artificial solid surface where there is very little interaction between the surface and the liquid in contact with it, slip would be appreciable for liquid flow. The analysis of the phenomenon was presented by Watanabe et al. (1999).

Because fluid slip occurs at highly water-repellent walls when the contact angle is about 150°, Watanabe et al. (1999) analyzed the friction factor of slip flow in a circular pipe. For a fully developed steady flow in a pipe, the Navier–Stokes equation can be written as

$$\frac{\mu}{r}\left[\frac{\mathrm{d}}{\mathrm{d}r}\left(r\frac{\mathrm{d}u}{\mathrm{d}r}\right)\right]=\left(\frac{\mathrm{d}P}{\mathrm{d}z}\right). \tag{3.37}$$

By integrating this equation, and owing to the physical consideration that the velocity must be finite at $r=0$,

$$u=\frac{r^2}{4\mu}\left(\frac{\mathrm{d}P}{\mathrm{d}z}\right)+C_1. \tag{3.38}$$

The constant C_1 is evaluated under the boundary conditions at the pipe wall: $r=a$, $u=u_\mathrm{s}$. Then, the slip velocity u_s is determined (Goldstein 1965) from a macroscopic point of view:

$$\tau_w=\mu\left(-\frac{\mathrm{d}u}{\mathrm{d}r}\right)_{r=r_0}=\beta u_\mathrm{s} \tag{3.39}$$

where β is the sliding coefficient. For the case of $\beta\to\infty$, Eq. (3.39) agrees with the no-slip condition. Consequently, this gives

$$C_1=\left(\frac{r_0}{2\beta}+\frac{r_0^2}{4\mu}\right)\left(\frac{-\mathrm{d}P}{\mathrm{d}z}\right) \tag{3.40}$$

and hence,

$$u=\left[\frac{r_0^2}{4\mu}\left(1-\frac{r^2}{r_0^2}\right)+\frac{r_0}{2\beta}\right]\left(\frac{-\mathrm{d}P}{\mathrm{d}z}\right). \tag{3.41}$$

The volume flow rate is

$$Q=\int_0^a 2\pi r u\,\mathrm{d}r=\frac{\pi r_0^4\Delta P}{8\mu L}\left(1+\frac{4\mu}{r_0\beta}\right) \tag{3.42}$$

where $(\Delta P/L)$ is the pressure gradient in a fully developed flow, and equals $(-\mathrm{d}P/\mathrm{d}z)$. The friction factor for laminar flow, λ, is

$$\lambda=\frac{64}{\mathrm{Re}}\frac{1}{1+\frac{4\mu}{r_0\beta}}. \tag{3.43}$$

Thus, in laminar flow with fluid slip, the friction factor is a function of not only the Reynolds number Re, but also the non-dimensional parameter $(\mu/a\beta)$. If the flow does not exhibit fluid slip, Eq. (3.43) gives $\lambda = 64/\mathrm{Re}$ on substituting $\beta \to \infty$ into the equation.

A series of experiments was presented by Ou et al. (2004), which demonstrate significant drag reduction for the laminar flow of water through micro-channels using hydrophobic surfaces with well-defined micron-sized surface roughness.

The difference between a hydrophobic surface and an ultrahydrophobic surface lies not in the surface chemistry, but in the micro-scale surface roughness. Ultrahydrophobic surfaces are actually very rough with large, micron-sized protrusions coming out of the surface. An optical micrograph of an ultrahydrophobic lithographically etched silicon surface is shown in Fig. 3.15. The equilibrium contact angles for each of these surfaces were found to be greater than 160°.

A schematic diagram of the physical model is shown in Fig. 3.16.

Average pressure drop reduction as a function of flow rate for a series of different surfaces in a micro-channel is shown in Fig. 3.17, where $\mathrm{Dr} = \frac{\left(\Delta P_{\text{no-slip}} - \Delta P\right)}{\Delta P_{\text{no-slip}}}$, ΔP is the experimentally measured pressure drop and $\Delta P_{\text{no-slip}}$ is the theoretical pressure drop prediction for flow over a no-slip surface at the same flow rate.

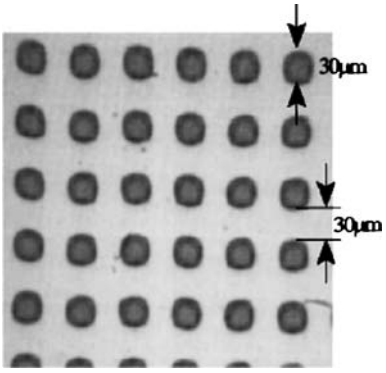

Fig. 3.15 Examples of ultrahydrophobic surfaces. Lithographically etched silicon surface patterned with 30 μm tall cubic micro-posts. Reprinted from Ou et al. (2004) with permission

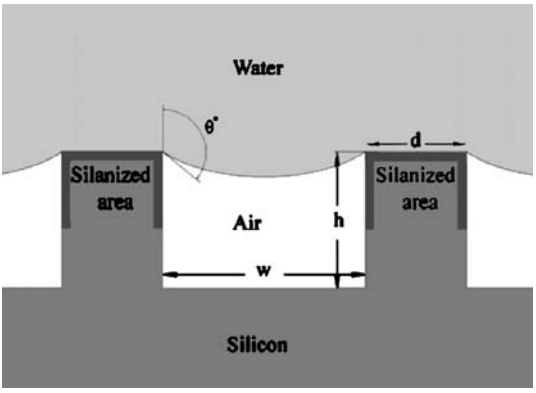

Fig. 3.16 Schematic diagram of a model for ultrahydrophobic drag reduction. A combination of surface hydrophobicity and roughness combine to allow water to stand away from the solid surface. Reprinted from Ou et al. (2004) with permission

The paper by Davies et al. (2006) reports results of a numerical investigation of the laminar, periodically repeating flow in a parallel-plate micro-channel with superhydrophobic walls. In particular, the influence of the Reynolds number and the vapor cavity size on the overall flow dynamics was explored. A schematic of the near-wall and cavity regions is shown in Fig. 3.18.

The walls exhibit micro-rib and cavity structures oriented perpendicular (transverse) to the flow direction and the walls are treated with a hydrophobic coating. Re-

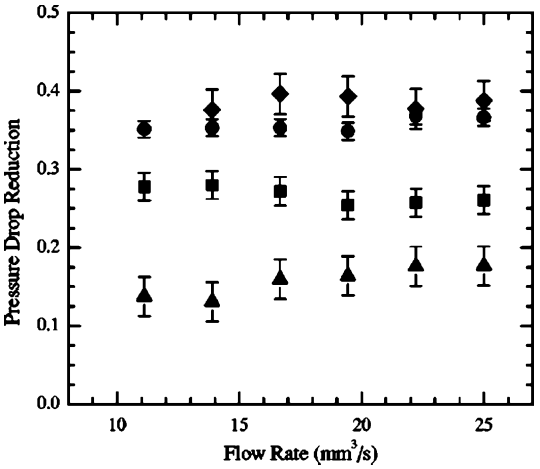

Fig. 3.17 Average pressure drop reduction as a function of flow rate for a series of different surfaces in a micro-channel having dimensions $W = 2.54$ mm, $H = 127$ μm, and $L = 50$ mm. The experimental data include a series of ultrahydrophobic surfaces with a regular array of square micro-posts with $d = 30$ μm with a spacing between micro-posts of $w = 15$ μm represented by *triangles* (▲), $d = 30$ μm and $w = 30$ μm represented by *squares* (■), $d = 30$ μm and $w = 60$ μm represented by *circles* (●), and $d = 30$ μm and $w = 150$ μm represented by *diamonds* (♦). Reprinted from Ou et al. (2004) with permission

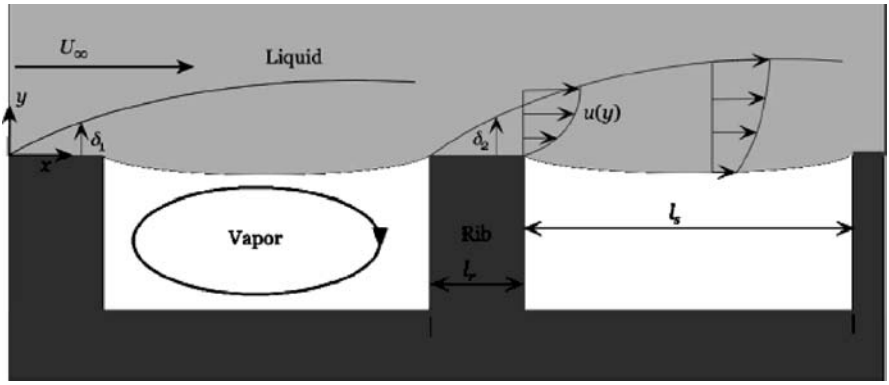

Fig. 3.18 Schematic of the near-wall and cavity regions for liquid flow over a superhydrophobic surface exhibiting micro-rib structures and flow perpendicular to the ribs

ductions in the frictional drag are greater as the cavity-to-rib length ratio is increased (increasing shear-free fraction) and as the channel hydraulic diameter is decreased.

The results also show that the normalized slip length and the average friction factor–Reynolds number product exhibit Reynolds dependence. Furthermore, the predictions reveal that the impact of the vapor cavity depth on the overall frictional resistance is minimal provided the depth of the vapor cavity is greater than 25% of its width.

Summary

Because most applications for micro-channel heat sinks deal with liquids, most of the former studies were focused on micro-channel laminar flows. Several investigators obtained friction factors that were greater than those predicted by the standard theory for conventional size channels, and, as the diameter of the channels decreased, the deviation of the friction factor measurements from theory increased. The early transition to turbulence was also reported. These observations may have been due to the fact that the entrance effects were not appropriately accounted for. Losses from change in tube diameter, bends and tees must be determined and must be considered for any piping between the channel plenums and the pressure transducers. It is necessary to account for the loss coefficients associated with single-phase flow in micro-channels, which are comparable to those for large channels with the same area ratio.

Internal pressure measurements would eliminate these effects. In addition to accounting for the losses outside the channel, it is also necessary to consider the pressure drop associated with developing flow in the entrance region of the channel.

The uncertainty of calculating the Poiseuille number from the measurements must be taken into account. The viscosity–pressure relationship of certain liquids (e.g., isopropanol, carbon tetrachloride) must be kept in mind to obtain the revised theoretical flow rate. The effect of evaporation from the collection dish during the mass flow rate measurement must be taken into consideration. The effect of evaporation of collected water into the room air may not be negligible, and due to the extremely low mass flow rates through the micro-channel this effect can become significant.

The main aim of the present chapter is to verify the capacity of conventional theory to predict the hydrodynamic characteristics of laminar Newtonian incompressible flows in micro-channels in the hydraulic diameter range from $d_h = 15$ to $d_h = 4{,}010\,\mu\text{m}$, Reynolds number from $\text{Re} = 10^3$ up to $\text{Re} = \text{Re}_{cr}$, and Knudsen number from $\text{Kn} = 0.001$ to $\text{Kn} = 0.4$. The following conclusions can be drawn from this study:

The comparison of experimental results accounting for effects discussed above to those obtained by conventional theory is correct when the experimental conditions were consistent with theoretical ones, and agrees well with Poiseuille flow predictions.

For single-phase fluid flow in smooth micro-channels of hydraulic diameter the Poiseuille number is independent of the Reynolds number. For single-phase gas flow in micro-channels of hydraulic diameter 16.6 to 4,010 μm, Knudsen number of Kn = 0.001−0.38, Mach number of Ma = 0.07−0.84, the experimental friction factor agrees quite well with theoretical one predicted for fully developed laminar flow.

The problem of transition to turbulence has been studied. The data for all channels showed no indication that a transition to turbulence began for Re up to 2,000. The behavior of the flow in micro-channels, at least down to 50 μm diameter, shows no difference with macro-scale flow. For smooth and rough micro-channels with relative roughness in the range of $k_s = 0.32-7\%$ the transition from laminar to turbulent flow occurs in the range of Reynolds number Re = 1,800−2,200, in full agreement with flow visualization and flow resistance data. These results support the standard findings that laminar flow is maintained for Re < 2,300. It is important to note that when the data from a given paper is examined independently, it often shows a consistent deviation from the theoretical predictions. However, when the data from many papers are summarized they are randomly scattered both above and below the standard predictions for large channels.

For flow of some kind of surfactant solutions (Habon G solutions at concentration 530 and 1,060 ppm) in the tube of $d = 1.07$ mm in the range of Reynolds number based on solvent viscosity Re = 10−450, the increase of pressure drop in adiabatic and diabatic conditions was observed compared to that of pure water.

Under certain conditions the energy dissipation may lead to an oscillatory regime of laminar flow in micro-channels. The relation of hydraulic diameter to channel length and the Reynolds number are important factors that determine the effect of viscous energy dissipation on flow parameters. The oscillatory flow regime occurs in micro-channels at Reynolds numbers less than Re_{cr}. In this case the existence of velocity fluctuations does not indicate change from laminar to turbulent flow.

One approach recently proposed reducing the pressure drop of liquids flowing in micro-channels by creating micro-ribs and cavities on the micro-channel walls. If these micro-rib/cavity structures are treated with a hydrophobic coating and the cavity size is small enough, the liquid flowing in the micro-channels wets only the surface of the ribs, and does not penetrate the cavities. The liquid thus forms a free surface meniscus in the cavity regions between the micro-ribs. The result is a reduction in the surface contact area between the channel walls and the flowing liquid, and a reduction in pressure drop up to 40% may be achieved.

References

Bailey DK, Ameel TA, Warrington RO, Savoie TI (1995) Single phase forced convection heat transfer in micro-geometries. In: Proceedings the 13th of Intersociety Energy Conversion Engineering Conference, San Diego, 20–25 August 1978. American Society of Mechanical Engineers, New York, pp 301–310

Bastanjian SA, Merzhanov AG, Xudiaev SI (1965) On hydrodynamic thermal explosion. Sov Phys Docl 163:133–136

Bayraktar T, Pidugu SB (2006) Characterization of liquid flows in micro-fluidic systems. Int J Heat Mass Transfer 49:815–824

Berg van den HR, Seldom ten CA, Gulik van der PS (1993) Compressible laminar flow in a capillary. J Fluid Mech 246:1–20

Brutin D, Tadrist L (2003) Experimental friction factor of a liquid flow in micro-tubes. Phys Fluids 15:653–661

Celata GP, Gumo M, Zummo G (2004) Thermal-hydraulic characteristics of single-phase flow in capillary pipes. Exp Thermal Fluid Sci 28:87–95

Celata GP, Morini GL, Marconi V, McPhail SS, Zummo G (2005) Using viscous heating to determine the friction factor in micro-channels: an experimental validation. In: Proceedings of ECI International Conference on Heat Transfer and Fluid Flow in Microchannel, Caste/Vecchio Pascoli, Italy, 25–30 September 2005

Celata GP, Cumo M, McPhail S, Zummo G (2006) Characterization of fluid dynamics behavior and channel wall effects in micro-tube. Int J Heat Fluid Flow 27:135–143

Cho YI, Hartnett JP (1982) Non-Newtonian fluids in circular pipe flows. Adv Heat Transfer 15:60–141

Cogswell FN (1981) Polymer melt rheology: a guide for industrial practice. Woodhead, Cambridge

Cui HH, Silber-Li ZH, Zhu SN (2004) Flow characteristics of liquids in micro-tubes driven by high pressure. Phys Fluids 16:1803–1810

Darbyshire AG, Mullin T (1995) Transition to turbulence in constant-mass-flux pipe flow. J Fluid Mech 289:83–114

Davies J, Maynes D, Webb BW, Woolford B (2006) Laminar flow in a microchannel with super hydrophobic walls exhibiting transverse ribs. Phys Fluids 18:087110

Duncan AB, Peterson GP (1994) Review of microscale heat transfer. Appl Mech Rev 47:397–428

Frank-Kamenetskii DA (1969) Diffusion and heat transfer in chemical kinetics, 2nd edn. Plenum, New York

Frenkel L (1946) Kinetic theory of liquids. Clarendon, Oxford

Gad-el-Hak M (1999) The fluid mechanics of microdevices. The Freeman Scholar Lecture. J Fluid Eng 121:5–33

Gad-el-Hak M (2003) Comments or critical view on new results in micro-fluid mechanics. Int J Heat Mass Transfer 46:3941–3945

Goldstein S (1965) Modern developments in fluid dynamics, vol 2. Dover, New York, pp 676–680

Gruntfest IJ, Young JP, Jhonson NL (1964) Temperatures generated by the flow of liquids in pipes. J Appl Phys 35:18–23

Guo ZY, Li ZX (2002) Size effect on micro-scale single phase flow and heat transfer. In: Proceedings of the 12th International Heat Transfer Conference, Grenoble, France, 18–23 August 2002

Guo ZY, Li ZX (2003) Size effect on micro-scale single-phase flow and heat transfer. Int J Heat Mass Transfer 46:149–159

Hagen G (1839) Über die Bewegung des Wassers in engen zylindrischen Rohren. Pogg Ann 46:423–442

Hao PF, Zhang XW, Yao FHe (2007) Transitional and turbulent flow in circular micro-tube. Exp. Thermal and Fluid Science 32:423-431

Harley JC, Huang Y, Bau HH, Zewel JN (1995) Gas flow in micro-channels. J Fluid Mech 284:257–274

Herwig H (2000) Flow and heat transfer in micro systems. Is everything different or just smaller. ZAMM 82:579–586

Herwig H, Hausner O (2003) Critical view on new results in micro-fluid mechanics: an example. Int J Heat Mass Transfer 46:935–937

Hetsroni G, Gurevich M, Mosyak A, Rozenblit R (2004) Drag reduction and heat transfer of surfactants flowing in a capillary tube. Int J Heat Mass Transfer 47:3797–3869

Hetsroni G, Zakin JL, Lin Z, Mosyak A, Pancallo EA, Rozenblit R (2001) The effect of surfactants on bubble grows, wall thermal patterns and heat transfer in pool boiling. Int J Heat Mass Transfer 44:485–497

Hetsroni G, Mosyak A, Pogrebnyak E, Yarin LP (2005) Fluid flow in micro-channels. Int J Heat Mass Transfer 48:1982-1998
Ho C-M, Tai Y-C (1998) Micro-electro-mechanical systems (MEMS) and fluid flows. Ann Rev Fluid Mech 30:579–612
Hsieh SS, Tsai HH, Lin CY, Huang CF, Chien CM (2004) Gas flow in long micro-channel. Int J Heat Mass Transfer 47:3877–3887
Hwang YW, Kim MS (2006) The pressure drop in microtubes and correlation development. Int J Heat Mass Transfer 49:1804–1812
Incropera FP (1999) Liquid cooling of electronic devices by single-phase convection. Wiley, New York
Jones OC (1976) An improvement in the calculation of turbulent friction factor in rectangular ducts. Trans ASME J Fluid Eng 98:173–181
Judy J, Maynes D, Webb BW (2002) Characterization of frictional pressure drop for liquid flows through micro-channels. Int J Heat Mass Transfer 45:3477–3489
Kandlikar SG, Joshi S, Tian S (2003) Effect of surface roughness on heat transfer and fluid flow characteristics at low Reynolds numbers in small diameter tubes. Heat Transfer Eng 24:4–16
Koo J, Kleinstreuer C (2004) Viscous dissipation effects in microtubes and microchannels. Int J Heat Mass Transfer 47:3159–3169
Leite RJ (1959) An experimental investigation of the stability of Poiseuille flow. J Fluid Mech 5:81–96
Lelea D, Nishio S, Takano K (2004) The experimental research on micro-tube heat transfer and fluid flow of distilled water. Int J Heat Mass Transfer 47:2817–2830
Li ZX, Du DX, Guo ZY (2003) Experimental study on flow characteristics of liquid in circular micro-tubes. Microscale Thermophys Eng 7:253–265
Lindgren ER (1958) The transition process and other phenomena in viscous flow. Arkiv für Physik 12:1–169
Loitsianskii LG (1966) Mechanics of liquid and gases. Pergamon, Oxford
Lumley JL (1969) Drag reduction by additives. Ann Rev Fluid Mech 1:367–384
Ma HB, Peterson GP (1997) Laminar friction factor in microscale ducts of irregular cross section. Microscale Thermophys Eng 1:253–265
Mala GM, Li D (1999) Flow characteristics of water in micro-tubes. Int J Heat Fluid Flow 20:142–148
Maynes D, Webb AR (2002) Velocity profile characterization in sub-diameter tubes using molecular tagging velocimetry. Exp Fluids 32:3–15
Morini GL (2004) Laminar-to-turbulent transition in microchannels. Microscale Thermophys Eng 8:15–30
Obot NT (1988) Determination of incompressible flow friction in smooth circular and noncircular passages. A generalized approach including validation of the century old hydraulic diameter concept. Trans ASME J Fluid Eng 110:431–440
Ou J, Perot B, Rothstein JP (2004) Laminar drag reduction in microchannels using ultrahydrophobic surfaces. Phys Fluids 16(12):4635–4643
Papautsky I, Brazzle J, Ameel T, Frazier B (1999) Laminar fluid behavior in micro-channels using micro-polar fluid theory. Sens Actuators 73:101–108
Peng XF, Peterson GP (1996) Convective heat transfer and friction for water flow in micro-channel structures. Int J Heat Mass Transfer 39:2599–2608
Peng XF, Wang BX (1998) Forced convection and boiling characteristics in micro-channels. In: Heat Transfer 1998 Proceedings of the 11th IHTC, Kyongju, Korea, 23–28 August 1998, vol 11, pp 371–390
Pfund D, Rector D, Shekarriz A (2000) Pressure drop measurements in a micro-channel. AIChE J 46:1496–1507
Plam B (2000) Heat transfer in microchannels. In: Heat Transfer and Transport Phenomena in Microscale. Banff Oct:54–64
Poiseuille JLM (1840) J Recherches experimentelles tubes de tris petits diameters. Comptes Rendus 11:961–967, 1041–1048

Qu W, Mala GM, Li D (2000) Pressure driven water flows in trapezoidal silicon micro-channels. Int J Heat Mass Transfer 43:353–364
Rands C, Webb BW, Maynes D (2006) Characterization of transition to turbulence in micro-channels. Int J Heat Mass Transfer 49:2924–2930
Ren L, Qu W, Li D (2001) Interfacial electrokinetic effects on liquid flow in micro-channels. Int J Heat Mass Transfer 44:3125–3134
Schlichting H (1979) Boundary layer theory. McGraw-Hill, New York
Sedov LI (1993) Similarity and dimensional methods in mechanics, 10th edn. CRC, Boca Raton
Shah RK, London AL (1978) Laminar flow forced convection in duct. Academic, New York
Shapiro AK (1953) The dynamics and thermodynamics of compressible fluid flow. Wiley, New York
Sharp KV, Adrian RJ (2004) Transition from laminar to turbulent flow in liquid filled microtubes. Exp Fluids 36:741–747
Sharp KV, Adrian R, Santiago J, Molho JI (2001) Liquid flows in micro-channels. In: CRC Handbook of MEMS. CRC, Boca Raton, pp 6.1–6.38
Tani I (1969) Boundary layer transition. Ann Review of Fluid Mech 1:169–196
Tso CP, Mahulikar SP (1998) The use of the Brinkman number for single phase forced convective heat transfer in micro-channels. Int J Heat Mass Transfer 41:1759–1769
Tso CP, Mahulikar SP (1999) The role of the Brinkman number in analysis flow transition in micro-channel. Int J Heat Mass Transfer 42:1813–1833
Tso CP, Mahulikar SP (2000) Experimental verification of the role of Brinkman number in micro-channels using local parameters. Int J Heat Mass Transfer 43:1837–1849
Tuckerman DB (1984) Heat transfer micro-structure for integrated circuits. Dissertation, Department of Electrical Engineering, Stanford University
Vargaftik NB, Vinogradov YK, Vargin VS (1996) Handbook of physical properties of liquids and gases. Pure substances and mixtures, 3rd augm. rev. edn. Begell House, New York
Virk PS, Mickley HS, Smith KA (1970) The ultimate asymptote and mean flow structure in Toms' phenomenon. ASME J Appl Mech 37:488–493
Warholic MD, Schmidt GM, Hanratty TJ (1999) The influence of a drag-reducing surfactant on a turbulent velocity field. J Fluid Mech 388:1–20
Watanabe K, Udagawa Y, Udagawa H (1999) Drag reduction of Newtonian fluid in a circular pipe with a highly water-repellent wall. J Fluid Mech 381:225–238
White FM (1994) Fluid mechanics, 3rd edn. McGraw-Hill, New York
Wu HY, Cheng P (2003) Friction factors in smooth trapezoidal silicon micro-channels with different aspect ratio. Int J Heat Mass Transfer 46:2519–2525
Wygnanskii IJ, Champagne FH (1973) On transition in a pipe. Part 1. The origin of puffs and slugs and the flow in a turbulent slug. J Fluid Mech 59:281–351
Xu B, Ooi KT, Wong NT, Choi WK (2000) Experimental investigation of flow friction for liquid flow in micro-channels. Int Comm Heat Transfer 27(8):1165–1176
Yang CY, Wu JC, Chien HT, Lu SR (2003) Friction characteristics of water, R-134a, and air in small tubes. Microscale Thermophys Eng 7:335–348
Zakin JL, Myska J, Chara Z (1996) New limiting drag reduction and velocity profile asymptotes for nonpolymeric additives systems. AIChE J 42:3544–3546
Zakin JL, Qi Y, Zhang Y (2002) In: Proceedings of 15th International Congress of Chemical and Process Engineering, CHISA 2002, Prague, Czech Republic, 25–29 August 2002
Zel'dovich JaB, Barenblatt GI, Librovich VB, Makhviladze GM (1985) Mathematical theory of combustion and explosion. Plenum, New York

Nomenclature

a	Side of a equilateral triangle
C^*	Ratio of $\mathrm{Po}_{\mathrm{exp}}/\mathrm{Po}_{\mathrm{theor}}$
c_p	Specific heat
d	Diameter
d_*	Characteristic size
E	Activation energy
$f = \dfrac{\lambda}{4}$	Fanning friction factor
h	Enthalpy, heat transfer coefficient
H	Side of a rectangle; depth of plane micro-channel
k	Thermal conductivity
k_s	Average height of surface roughness
L	The length of the micro-channel
$\overline{L} = L/d_*$	Dimensionless length
m	Mass flow rate
P	Pressure
r	Current radius
r_0	Inner radius
R	Universal gas constant
T	Temperature
t	Time
U	Average velocity
u	Longitudinal component of velocity
u'	rms velocity fluctuation
u_s	Slip velocity
u_*	Friction velocity
u_k	Velocity at the top of the roughness element
x, y, z	Cartesian coordinates
$\mathrm{Ec} = \frac{U^2}{2C_p\Delta T}$	Eckert number
$\mathrm{Kn} = \frac{\overline{\lambda}}{d_h}$	Knudsen number
$\mathrm{Ma} = \frac{U}{U_{\mathrm{sound}}}$	Mach number
$\mathrm{Po} = \lambda\mathrm{Re}$	Poiseuille number
$\mathrm{Pr} = \frac{\nu}{\alpha}$	Prandtl number
$\mathrm{Re} = \frac{Ud_h}{\nu}$	Reynolds number
$\mathrm{Re}_k = \frac{u_k k_\mathrm{s}}{\nu}$	Reynolds number based on average height of surface roughness

Greek Symbols

α	Thermal diffusivity
β	Sliding coefficient
α, β	Semi-axis of the ellipse
ΔT	Temperature difference
ΔP	Pressure drop
δ	Uncertainty, characteristic size
ε	Channel aspect ratio
η	Dimensionless radius
θ	Dimensionless temperature, variable
λ	Friction factor
$\overline{\lambda}$	Mean free path
μ	Dynamic viscosity
μ_m	Viscosity determined by roughness – viscosity model
ν	Kinematic viscosity
ξ	Height to width ratio, variable
ρ	Density
τ	Shearing stress at a wall
Φ	Energy dissipation
χ	Variable

Subscript

ac	Actual
av	Average
cr	Critical
ef	Effective
exp	Experimental
h	Hydraulic
in	Inlet
lam	Laminar
max	Maximum
out	Outlet
sh	Shear
theor	Theoretical
w	Wall
wat	Water